Master's dissertation

The mysterious population of globular clusters of the ultra-diffuse galaxy MATLAS-2019

Sergio Guerra Arencibia

Supervisor: Mireia Montes Quiles
Co-supervisor: Ignacio Trujillo Cabrera

La Laguna, July 6, 2023

Abstract

This master's disertation aims to analyze the Globular Cluster (GC) system of MATLAS-2019, an Ultra Diffuse Galaxy (UDG). The importance of this study lies in the controversial number of GCs of this galaxy, as recent scientific publications do not agree on its population size. Therefore, the intention of this work is to clarify the number of GCs of the galaxy. A precise understanding on how many GCs the galaxy has will allow us to better understand the origin and nature of these UDGs.

This study will take advantage of multiwavelength observations to obtain the cleanest sample of GC candidates. We will use the spatial resolution of the Hubble Space Telescope to obtain a preliminar catalogue of GC candidates. The main parameters for this initial selection are effective radius, ellipticity and magnitude. Then, a two-colour selection is performed to further discriminate between GCs and contaminants. The selection criteria is based on the properties of bona fide GCs from the literature as well as the spectroscopically confirmed GCs of MATLAS-2019.

A total of 28$\pm$2 globular clusters are identified. This result is in agreement with other estimations of the GC population of the galaxy. These results support the scenario in which ultra diffuse galaxies are dwarf galaxies that have undergone some processes that gives them the UDGs characteristics, favoring conventional explanations for their origin rather than more exotic hypotheses.

Palabras clave: Globular Clusters, Ultra diffuse galaxies, catalogues, dwarf galaxies

Resumen

El presente Trabajo Final de Máster tiene como principal objetivo el estudio, análisis y caracterización del sistema de cúmulos globulares de la galaxia MATLAS-2019, que se encuentra en la línea de visión del grupo NGC 5846. MATLAS-2019 es una galaxia enana de bajo brillo superficial ($\mu(g,0) \approx 24.8 \pm 0.1$, Forbes et al. 2019), perteneciente a la categoría de Galaxias Ultra Difusas (por sus siglas en inglés, UDGs). Esta categoría de galaxias enanas ha sido acuñada muy recientemente por van Dokkum et al. (2015), caracterizándose por su bajo brillo superficial ($\mu(g,0) \gtrsim 24$ mag arcsec^{-2}) y su gran radio efectivo ($r_e \gtrsim 1.5$ kpc). En los últimos años, las Galaxias Ultra Difusas han despertado gran interés en la comunidad científica debido a sus peculiares propiedades y a que nos abren la puerta a estudiar la formación de galaxias a bajas masas.

La existencia de estas Galaxias Ultra Difusas desafía nuestros modelos de formación de galaxias, dado que actualmente estos modelos no permiten explicar con certeza su origen y naturaleza. ¿Son galaxias enanas que, por una falta de formación estelar en los últimos tiempos o por algún otro tipo de proceso, han obtenido estas características? ¿O iban a ser galaxias más masivas que fallaron en algún punto de su desarrollo, quedándose como galaxias extendidas pero con muy poco brillo?

Para tratar de dar respuesta a estas cuestiones debemos estudiar las propiedades de las UDGs, para ver si se asemejan a las de otras galaxias enanas o si realmente son un tipo de objeto con características diferentes. Una de las principales propiedades que nos ayudarán a discernir el origen de las galaxias ultra difusas es la masa de sus halos de materia oscura. Si son galaxias enanas, sus halos de materia oscura debe ser similares a los halos de otras galaxias de este mismo tipo, pero si son galaxias masivas fallidas deben de habitar halos de materia oscura mucho más masivos que los correspondientes a galaxias enanas.

De esta manera, el estudio del número de cúmulos globulares que contiene una galaxia adquiere importancia, al estar relacionado linealmente (al menos para las galaxias "usuales") con la masa total de la galaxia. Esto se conoce como la relación Cúmulos globulares - Halo de materia oscura (comúnmente conocida en inglés como *globular cluster-dark matter halo relation*).

El estudio de los cúmulos globulares de MATLAS-2019 también es de especial relevancia, dado que actualmente existe discrepancia en la cantidad de cúmulos globulares que tiene esta galaxia. Diferentes autores en los últimos años han propuesto diferentes abundancias para este sistema, no quedando claro si la población de cúmulos globulares consta de alrededor de 25 objetos (Müller et al., 2021) o de más del doble (Danieli et al., 2022). Aclarar esta cuestión nos permitirá saber si la galaxia dispone de un sistema de cúmulos globulares abundante pero esperado o, si por el contrario, verdaderamente posee una población atípica.

Así pues, en este trabajo se realizará un estudio de la galaxia para estimar la cantidad de cúmulos globulares, tratando así de inclinar la balanza respecto al debate existente. Con el fin de obtener resultados más fiables, se llevará a cabo un estudio más completo de esta galaxia, usando más datos y parámetros de los que han sido utilizados en trabajos anteriores. Dado que la distancia a la galaxia no está bien definida, ya que algunos autores la situan sobre 21 Mpc y otros alrededor de 26 Mpc, se realizará el análisis para ambas distancias.

Los datos de los que se dispone son imágenes del telescopio espacial Hubble (HST) en tres filtros diferentes (*F475W*, *F606W* y *F814W*). Los datos de *F475W* y *F606W* provienen del instrumento Wide Field Camera 3 (WFC3) con un tiempo de exposición de aproximadamente 2350 segundos, mientras que los datos de F814W son del instrumento Advanced Camera for Surveys (ACS) con una exposición de aproximadamente 1000 segundos.

Para llevar a cabo la identificación de cúmulos globulares se realizará, en primer lugar, la construcción de un catálogo que contenga todas las fuentes posibles del campo. Dado que se dispone de datos en tres filtros diferentes, se construirán los cátalogos de cada imagen y posteriormente se combinarán en un catálogo final del campo. Para la construcción de los catálogos y su fotometría correspondiente se empleará el software *SExtractor*.

La selección de los cúmulos globulares candidatos se realizará mediante el filtrado del catálogo obtenido. Este filtrado se llevará a cabo en dos etapas. En primer lugar, se aplicará un filtrado basado en radio efectivo, elipticidad y magnitud. Posteriormente se realizará un segundo filtrado basado en el color. Los estudios realizados hasta ahora han dispuesto de un único color, pero en nuestro caso, dado que se disponen de tres filtros diferentes podemos obtener dos colores. Esto es una gran ventaja a la hora de discernir si una fuente es un cúmulo globular o no, puesto que usando dos colores exploraremos mejor la distribución espectral de energía de las fuentes, pudiendo así eliminar más contaminantes.

Los criterios empleados para la selección de cúmulos globulares se obtendrán en base a dos fuentes de información. La primera es un análisis de cúmulos globulares de la literatura que ya han sido identificados y caracterizados tanto en la Vía Láctea (Harris, 2010) como en galaxias enanas cercanas (Georgiev et al., 2009). La segunda se trata del estudio de once cúmulos globulares que han sido confirmados espectroscópicamente en MATLAS-2019 (Müller et al., 2020). Mediante la combinación de estos dos análisis, estudiando cuales son los rangos de valores típicos de radio efectivo, elipticidad, magnitud y color para un cúmulo globular, se establecen los criterios para determinar si una fuente puede ser considerada un cúmulo globular o no.

Una vez completado el proceso de filtrado, se obtiene que la población de cúmulos globulares de la galaxia MATLAS-2019 consta de 28 ± 2. A lo largo del trabajo se lleva a cabo un análisis de estos cúmulos globulares candidatos, estudiando su distribución espacial, su distribución de radios efectivos, su función de luminosidad (GCLF) y su distribución radial.

Además, la función de luminosidad de los cúmulos globulares encontrada sitúa a la galaxia a una distancia de aproximadamente 21 Mpc. Si la galaxia siguiera la relación entre el número de GCs y la masa del halo de materia oscura, entonces la masa de su halo sería aproximadamente $1.0 \times 10^{11} M_{\odot}$.

Resulta interesante destacar que la distribución de los cúmulos globulares en torno a la galaxia es notablemente asimétrica, a pesar de que el cuerpo difuso de la galaxia no presenta esta característica. Un estudio adicional sería necesario para determinar si esta disposición es arbitraria o si hay algún proceso subyacente responsable.

Una vez expuestos los resultados obtenidos en este trabajo, estos son discutidos y comparados con los resultados que otros autores obtienen del sistema de cúmulos globulares de la galaxia. Como se mencionó anteriormente, existe cierta discrepancia respecto a cuántos cúmulos globulares tiene la galaxia, y el estudio presentado aquí parece inclinar la balanza hacia que MATLAS-2019 tiene en torno a 28 cúmulos globulares.

La principal implicación de los resultados encontrados es que MATLAS-2019 posee un sistema de cúmulos globulares comparable a las poblaciones de otros tipos de galaxias enanas. Esto favorece el escenario en el que las Galaxias Ultra Difusas son galaxias enanas que mediante ciertos procesos (e.g., ausencia de formación estelar reciente, interacciones de marea) obtuvieron las características que manifiestan actualmente, constituyendo la región de bajo brillo superficial y gran radio efectivo de una abundante población de galaxias enanas.

Más estudios deben ser realizados para seguir desentrañando el origen de las galaxias ultra difusas, pero al menos MATLAS-2019 parece albergar un sistema de cúmulos globulares acorde con el de una galaxia enana.

Contents

Chapter 1

Introduction

Ever since humans learned about the existence of galaxies, they have wondered about their formation and structure. This is a question that, to this day, has not been resolved, or at least not completely. Galaxy formation and structure is a subject as important as complex for modern astrophysics.

The importance of studying and understanding galaxies does not need any kind of justification, being interesting objects of study in their own right. Nevertheless, it is thanks to the study of galaxies, which exist and are observable in great amount over a large number of distances and time scales, that we are better able to understand the structure and evolution of the universe itself.

Galaxy formation and evolution encompasses a large amount of different fields. In a very general way, we can catalogue this knowledge in three main groups: Cosmology, initial conditions and physical processes (Mo et al., 2010). The study that will be carried out is related to galaxy formation and evolution itself, but specially it is related to the cosmological part. The current cosmological framework is known as Lambda Cold Dark Matter (ΛCDM). It characterizes the scenario in which galaxy formation and evolution occurs.

The ΛCDM model has two main characteristics which are already indicated in its name. First the letter Λ, which represents the cosmological constant, associated with dark energy, needed to explain the accelerating expansion of the universe. Secondly, the letters CDM stand for Cold Dark Matter, the component of the cosmological framework to which this study is related. It is called *cold* because it moves slowly compared with the velocity of light (as opposed to *hot* dark matter) and *dark* due to its apparent absence of electromagnetic interactions. To this date, we do not know exactly what it is and what specific properties dark matter has, but it is thought to be responsible of $\sim 21\%$ of the energy density of the universe. It is also fundamental because without it the primordial gas would not be able to collapse and form galaxies because not enough gravity forces would be present.

Dark matter does not interact (or if it does, it will only very weakly) electromagnetically, instead its interactions are mainly gravitational. This makes DM extremely complicated to study and forces us to try to understand it through its effect on the visible matter that we can study through the current available techniques: baryonic matter. Thus, studying galaxies, their properties, their formation and evolution is the main way of achieving one of the great scientific objectives of modern times, that is, obtain constraints on the dark matter nature.

There are a vast number of different types of galaxies, from dwarf galaxies, which are composed of a few billion stars ($n_{stars} \sim 10^9$) or less, to bigger galaxies like the Milky way which are composed of hundreds of billions of stars ($n_{stars} \sim 10^{11}$). In any case, the ones that will have our attention in this study are dwarf galaxies.

Dwarf galaxies are the most numerous galaxies in the universe. They have a crucial importance for various reasons, one of the main ones being that dwarf galaxies exist in a mass range where models and observations do not coincide. These disagreements between observations and models consist in the fact that we observe far fewer dwarf galaxies than expected by models and simulations. This is known as the Dwarf Galaxy Problem or Missing Satellite Problem (MSP), and having a better understanding of this type of galaxies will allow us to obtain answers to this problems and improve our models.

Another important characteristic of dwarf galaxies is that they are thought to be the most dark matter dominanted objects (e.g., Strigari et al. 2008; McGaugh and Wolf 2010) making them an excellent laboratory for studying and obtaining constraints about this elusive component of the universe. Furthermore, not only are dwarf galaxies dominated by dark matter, but the least massive of their kind can also have the most pristine dark matter halos. This is a consequence of its low mass and, therefore, less contribution of the different sources of feedback. As there is less feedback the dark matter halos are less disturbed, maintaining better its original characteristics.

There are different types of dwarf galaxies (dwarf irregulars, dwarf ellipticals, dwarf spheroidals, etc...), but those that are important for the present work are the Ultra Diffuse Galaxies (UDGs). This category of dwarf galaxies have been known from more than 30 years, but they have become popular recently thanks to the work by van Dokkum et al. (2015).

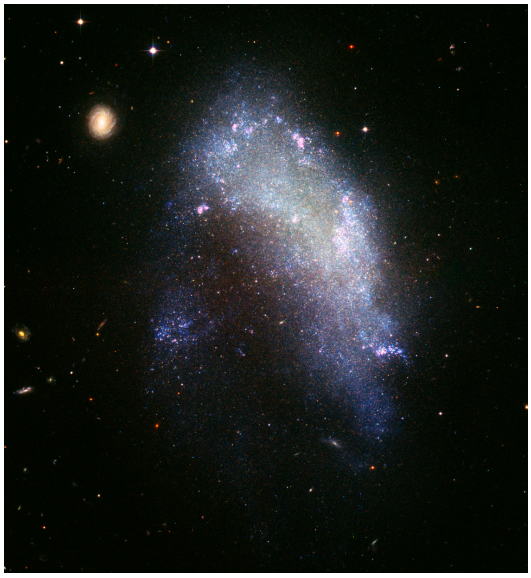

Figure 1.1: NGC 1427A as an example of dwarf irregular.

UDGs have a really low central surface brightness ($\mu(g,0) \gtrsim 24$ mag arcsec^{-2}) and a large effective radius ($r_e \gtrsim 1.5$ kpc). The origin of these galaxies is currently a hot topic (see brief review in Trujillo 2021), where the two main hypothesis are that either they are normal dwarf galaxies that underwent some physical process that modified its properties (e.g., no recent star formation, tidal interactions, high initial halo spins, stellar feedback), or they were going to be massive galaxies that at some point stopped forming stars for some reason (being a failed galaxy embedded in a massive dark matter halo) (Saifollahi et al., 2022).

To clarify the nature of the UDGs is necessary to know if their properties are similar to other dwarf galaxies or not. One of the most important and interesting properties to study is the massiveness of its dark matter halo, because knowing how large their halos are will give us a valuable insight about if they are failed galaxies or not.

There are different methods for measuring the amount of DM that a galaxy has, for example weak lensing, velocity disperion or rotation curve. Another empirically-based possibility is inferring the dark matter using the number of globular clusters in the galaxy (N_{GC}), a quantity that is linearly related with the total mass of the galaxy, a relation which is known as *Globular cluster-Halo mass relation*.

The Globular cluster-Halo mass relation is an empirical connection found between the N_{GC} and the total mass of the galaxy. It is a really useful and convenient relation since the GC are bright and compact objects, detectable even at long distances and the relationship holds from halo masses of $\sim 10^9 M_\odot$ to $\sim 10^{14} M_\odot$ (Forbes et al., 2018). The most surprising thing of the relation is that it tells us about an intrinsic connection between Globular clusters and Dark matter.

It is not clear the origin of this relation. The most tempting explanation is to assume a initial relationship between the stellar mass that forms in the globular clusters and the mass of the halo, (Choksi and Gnedin, 2019). Another posibility is that such relationship is due to the repeated and continuous merging of galaxies, this is, due to the central limit theory (El-Badry et al., 2018). This explanation, however, although attractive for massive galaxies is more unlikely for dwarf galaxies. Of course, to obtain an explanation for this relation is important to check and enhance the current galaxy formation models.

The aim of this work is to find a clean sample of GC candidates in a hotly debated UDG. There is disagreement in the scientific community regarding the number of GCs of the galaxy. Therefore, the ultimate goal of this work is to perform a thorough study and obtain the $N_{\rm GC}$. Obtaining this information about the GC system of the galaxy can help us discern between the proposed mechanism for the formation of this galaxy and, this way, earn valuable information for our understanding of galaxy formation.

The galaxy of interest is on the line of sight of the NGC 5846 group and has multiple names due to how it has been detected and catalogued. These are NGC 5846-156 (Mahdavi et al., 2005), NGC 5846_UDG1 (Forbes et al., 2019) and MATLAS-2019 (Habas et al., 2020). For simplicity, the name MATLAS-2019 will be used in this study.

The galaxy is located at RA: 15:05:20.34, Dec: +01:48:44.9. The total apparent magnitude in the g band is around 18.0 mag and its central g band surface brightness ($\mu(0, g)$) is 24.8 $\pm$ 0.1 mag/arcsec^2 (Forbes et al., 2019). Figure 1.2 is taken from Danieli et al. (2022) and shows a *F475W* - *F606W* combined color image of the galaxy seen from the Hubble Space Telescope (HST), WFC3 instrument.

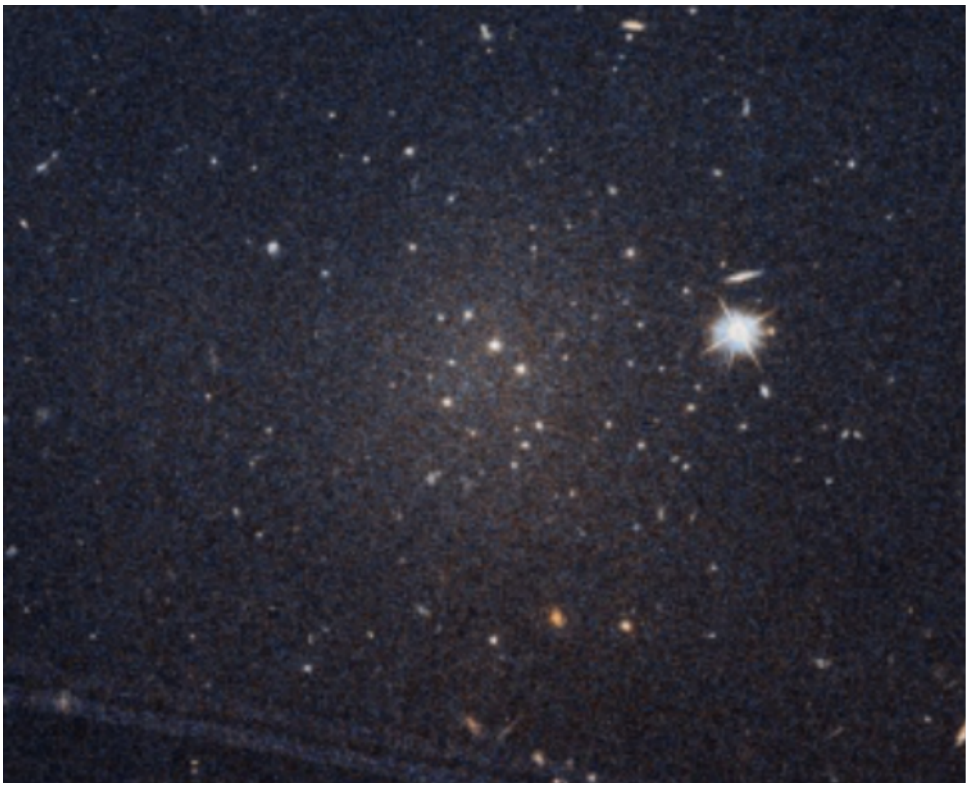

Figure 1.2: MATLAS-2019 seen from the Hubble Space Telescope, WFC3 instrument. Image taken from Danieli et al. (2022).

Chapter 2

Background and objectives

Background

In recent years, MATLAS-2019 has been the subject of multiple studies and debates (e.g. Müller et al. 2021; Danieli et al. 2022). Curiously, this object had been identified as a *Very Low Surface Brightness* (VLSB) galaxy, with the name NGC 5846-156 by Mahdavi et al. (2005). Still, this first identification did not attract special attention. Also, it is worth mentioning that the effective radius measured in this study fell slightly below the currently assumed UDG effective radius limit (i.e. 1.5 kpc) at an assumed distance of 26 Mpc.

Ten years later, van Dokkum et al. (2015) coined the UDG classification and galaxies with these characteristics began to be in the spotlight. This way, MATLAS-2019 was identified as a UDG by two different surveys (VEGAS and MATLAS) some years ago (Forbes et al., 2019; Habas et al., 2020).

In the images, MATLAS-2019 stands out for its apparently large number of globular clusters. In the same article in which Forbes et al. identifies MATLAS-2019 as an UDG, a superficial analysis (based on one image photometry and distribution of the sources) is made and 20 GCs are found as a lower limit to the total GC system. This number is astonishing as the turn over magnitude of the Globular cluster luminosity function (GCLF) ($m_g \approx 25$ mag) is not even reached (assuming this time a distance of around 25 Mpc). In a follow-up study, Forbes et al. (2020) uses this information to estimate the GC system count of the galaxy around 45.

Due to this finding, other studies about the GC population of the galaxy have been carried out. First, Müller et al. (2020) performed a spectroscopic study of the galaxy with the integral field spectrograph MUSE (Multi-Unit Spectroscopic Explorer). In this analysis a total of 11 GCs are spectroscopically confirmed, concluding a real lower limit to the population. This means that MATLAS-2019 has at least 11 GC. Knowing the existence of these 11 confirmed globular clusters, a couple of studies have been done trying to identify the total GC population.

Müller et al. (2021) studied MATLAS-2019 using two bands from the Hubble Space Telescope (HST) with the Advanced Camera for Surveys (ACS) instrument. A total of 26 ± 6 globular clusters candidates were found. This is a large GC population for a dwarf galaxy but still reasonable for what is expected. Although the previous distance measurements for the group indicate a distance around 26 Mpc, Müller et al. finds that a closer distance of around 21 Mpc is estimated from the Globular Cluster Luminosity Function (GCLF) that is obtained.

Later, Danieli et al. (2022) performed another study using two different bands from the HST with the Wide Field Camera 3 (WFC3) instrument. A globular cluster selection based on photometry and the Full Width Half Maximum of the sources is applied, finding a total of 54 ± 9 globular clusters. This is a really large population that challenges our understanding of galaxy formation. The distance associated with these results is 26.5 Mpc.

Currently the total number of globular clusters that MATLAS-2019 has still remains uncertain. It is also not clear the distance to the galaxy. Clarifying whether MATLAS-2019 has an extraordinary GC population will let us know whether it fits in our current understanding of galaxy formation or we have to update and modify our knowledge.

Objectives

The main goal of this study is to identify the globular clusters of MATLAS-2019, this is, characterize its globular cluster population. For that, a thorough study of the currently available data will be performed, aiming to obtain reliable results that shed some light on the current debate.

To try to obtain reliable results and to provide new and valuable information to the previous studies, a bigger amount of parameters will be included in the analysis. A globular cluster selection based on magnitude, ellipticity, effective radius and colours will be performed. Furthermore, unlike previous analyses, data from three filters is available, so two colours will be used to select candidates.

The first task will be to perform a study of the already identified and characterized globular clusters in our galaxy and in other dwarf galaxies. This way, the properties of these GCs are used to infer the expected properties of the GCs of MATLAS-2019 in the HST observations. we work under the assumption that the GCs of MATLAS-2019 are similar to local or nearby dwarf galaxies GCs.

After that, the detection software SExtractor is used in order to build an accurate catalogue of the galaxy. This is a really important step of the work because the quality of the catalogue will condition the whole analysis that will be performed later. Following this line of thought, the decisions regarding the creation of the catalogue (this is, the decision on the values of the selection parameters) are studied in detail and verified in different ways. Regarding the catalogue, is important to mention that all the magnitudes are given in the AB magnitude system. Once the catalogue is made, an analysis of the spectroscopically confirmed globular clusters is performed. This will provide us information about the specific characteristics of the GCs of this galaxy.

Putting together the information of the study of already identified GC and the information of the confirmed GCs, a selection criteria for the different parameters (effective radius, ellipticiy, magnitude and colours) will be decided. To make sure that no potential globular cluster candidates are lost, the criteria applied will be quite broad.

Applying this criteria to the sources of the catalogue will result in a population of globular cluster candidates. Finally, an analysis of the globular cluster candidates is done, the obtained results will be discussed and placed in the context of the current existing debate.

Summarizing, a schematic view of the main tasks is as follows:

1. Study of local and dwarf galaxies GCs.
2. Creation of the catalogue.
3. Study of the spectroscopically confirmed GCs.
4. Definition of the criteria that will be applied to select GCs.
5. Obtention of MATLAS-2019 GC population.
6. Analysis, discussion and contextualization of obtained results.

Chapter 3

Analysis

3.1 Reference globular clusters analysis

Before working and analyzing our data, it is important to do some research about the objects that we are going to study. These objects are the globular clusters.

There are a lot of references about globular clusters, one of the most important is the Milky Way globular cluster catalogue by Harris (2010). This data was published for the first time in 1996, although some updates have been done to the data and the version used here is the one from 2010. This data contains different parameters for 157 globular clusters. Also, an important compilation of GCs in dwarf galaxies has been made by Georgiev et al. (2009). This time the data contains parameters for 175 objects.

Both catalogs will be reviewed. Harris' catalog is interesting due to its completeness, which is a result of its vicinity. Additionally, Georgiev's catalog is noteworthy for including objects from dwarf galaxies, which are the type of galaxies that concerns us. The main parameters that we will study are absolute magnitude, effective radius and ellipticity.

3.1.1 Magnitudes

The first parameter that will be studied is the absolute magnitude. The magnitude distribution of GCs, this is, the Globular Cluster Luminosity Function (GCLF) appears to be universal (Rejkuba, 2012) across GCs of many different galaxy types. It peaks at a constant magnitude and has a constant dispersion. This characteristic of the globular clusters populations helps us to study them and also it has been a valuable distance indicator since the 1970-ies.

Usually the GCLF is approximated with a gaussian, peaking at $M_V \approx -7.6$ and with a certain width which is typically around 1 or 1.2 magnitudes, as it is described in a lot of studies (e.g., Richtler 2003; Rejkuba 2012).

For academic and completeness purposes the magnitude distribution of the Harris and Georgiev globular clusters data will checked. Figure 3.1 shows the magnitude distributions of the data. It is reasonable for both cases a Gaussian approximation, peaking at $M_V \approx -7.6$ and having similar standard deviations around one magnitude.

To be aware of what are we looking at, all the globular clusters in the Harris catalogue are from the Milky Way, but Georgiev's globular clusters data comes from different dwarf galaxies. It is also important to say that the Georgiev's data has an artificial cut-off at faint magnitudes due to the criteria that they use to accept a sources as globular clusters.

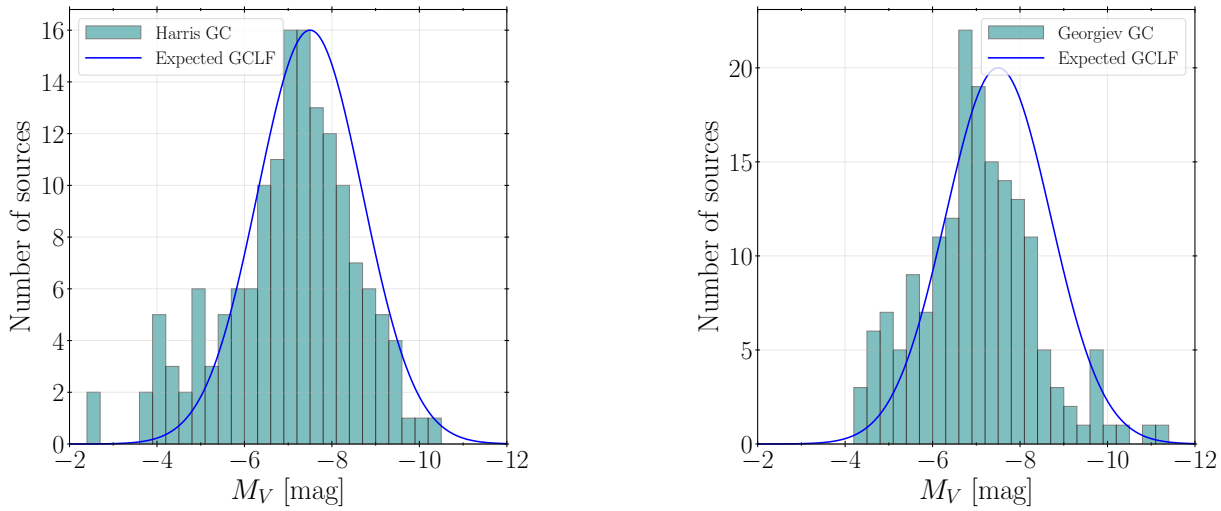

Figure 3.1: Magnitude distribution of globular clusters in Harris (left) and Georgiev (right) data. A Gaussian distribution (blue line) centered in $M_V = -7.6$ and with a width of 1.2 is a reasonable fit to the data.

3.1.2 Effective radius

The effective radius of the globular clusters is an important parameter for our study. We will use this value to perform aperture photometry to the globular clusters and also to decide if an object can be a globular cluster or not.

Three different measures of globular clusters radius are typically used: The core radius (where the surface brightness has fallen to half its central value), the effective radius (radius of a circle that contains half of the luminosity) and the tidal radius which is the outer limit of the cluster (where the stars are stripped by the tidal field of its host galaxy) (Binney and Tremaine, 2008). In the literature the effective radius is generally used and that measurement will be used here too.

We have plotted the distribution of effective radius of both catalogues to explore the range of this parameter. These plots can be seen in figure 3.2. In both data sets the majority of globular cluster (89% of them) are in the range of 0 to 10 parsecs. There are some larger objects, and although it is well known that there are globular cluster which can be considerably large (e.g. Pal 14 and NGC2419 in the Milky Way), it is not their typical radius.

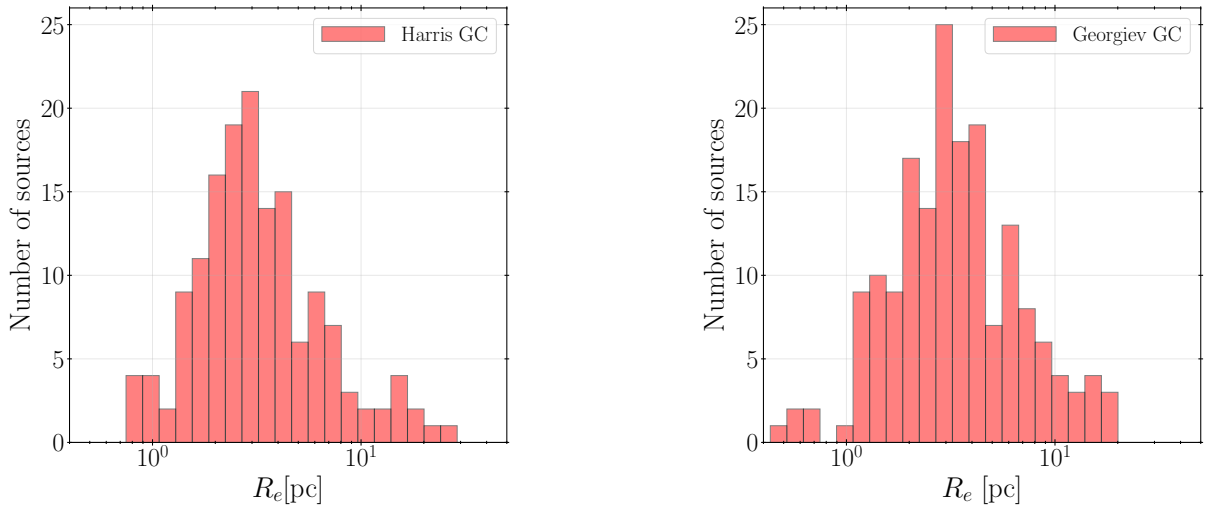

Figure 3.2: Effective radius distribution of globular clusters in Harris (left) and Georgiev (right) data. There are some big globular clusters (bigger than a 10 parsecs) but most of them (89% of the objects) are between 0 and 10 pc.

To characterize the average property of a representative globular cluster, we have derived the average properties (performing a sigma-clipping selection and a statistical study) for both catalogues. In the Harris' catalogue the mean effective radius is 3.5 pc with a standard deviation of around 2.3 pc. In Georgiev's data a mean effective radius of 3.6 pc and a standar deviation of 2.2 pc is found.

Assuming that both samples are representative subsets of the larger population, the standard error is computed, obtaining an error of 0.18 pc for Harris' data and 0.16 pc for Georgiev's. This shows that the effective radius is the same within the uncertainty. On what follows, we use $R_e = 3.6$ pc as the typical effective radius of a GC.

We have also explored whether there is some relation between effective radius and luminosity. This is an important thing to know for analyzing the future results that will be obtained and for getting rid of possible biases. In figure 3.3 it can be seen that there is no correlation between M_V and R_e. That is, GCs are not larger when they are more luminous (i.e. massive).

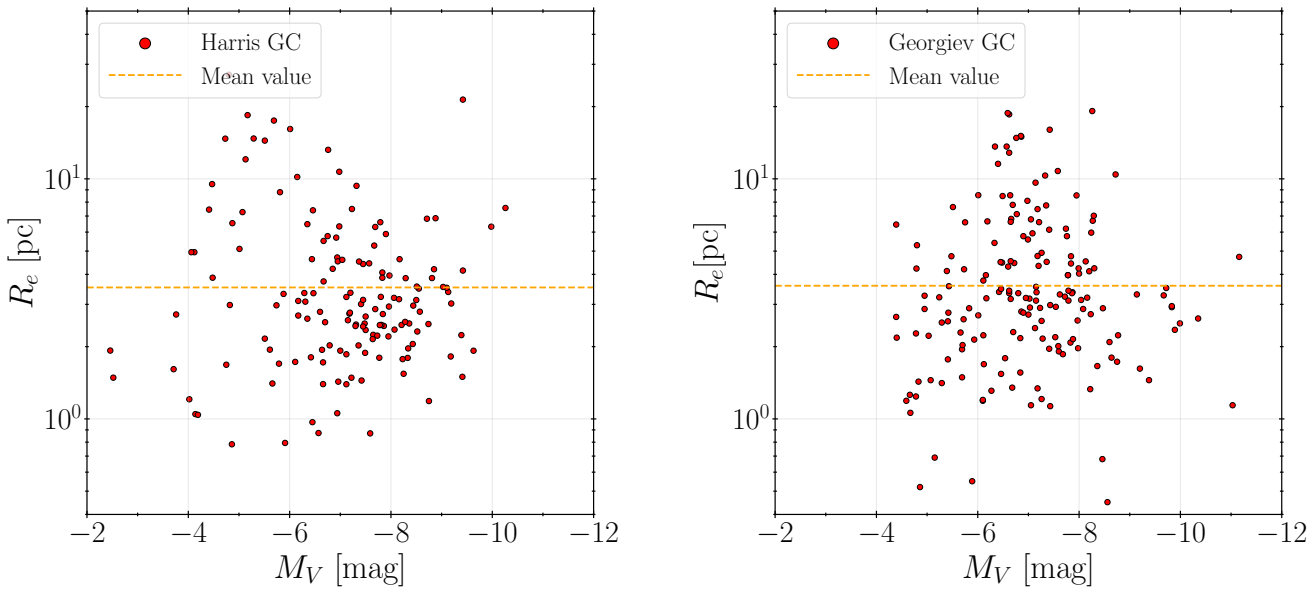

Figure 3.3: Absolute magnitude in V against effective radius of globular clusters in Harris (left) and Georgiev (right) data. No relation between effective radius and size is found.

3.1.3 Ellipticity

The last parameter that will be studied is the ellipticity. Globular clusters are gravitationally bound objects and therefore are expected to follow a spherical configuration. This is true as long as the object is not affected by a tidal field. Also, the measurements are not perfect and some ellipticity is usually measured. Checking what is the ellipticity measured in the two catalogues will help us to define a range of possible ellipticities for globular clusters.

In figure 3.4 the histogram of the ellipticities for Harris' and Georgiev's data is shown. Most of the globular clusters (around 94%) have ellipticites between 0.0 and around 0.20. There are some objects with higher ellipticies, which may be due to measurement inaccuracies or objects under tidal effects.

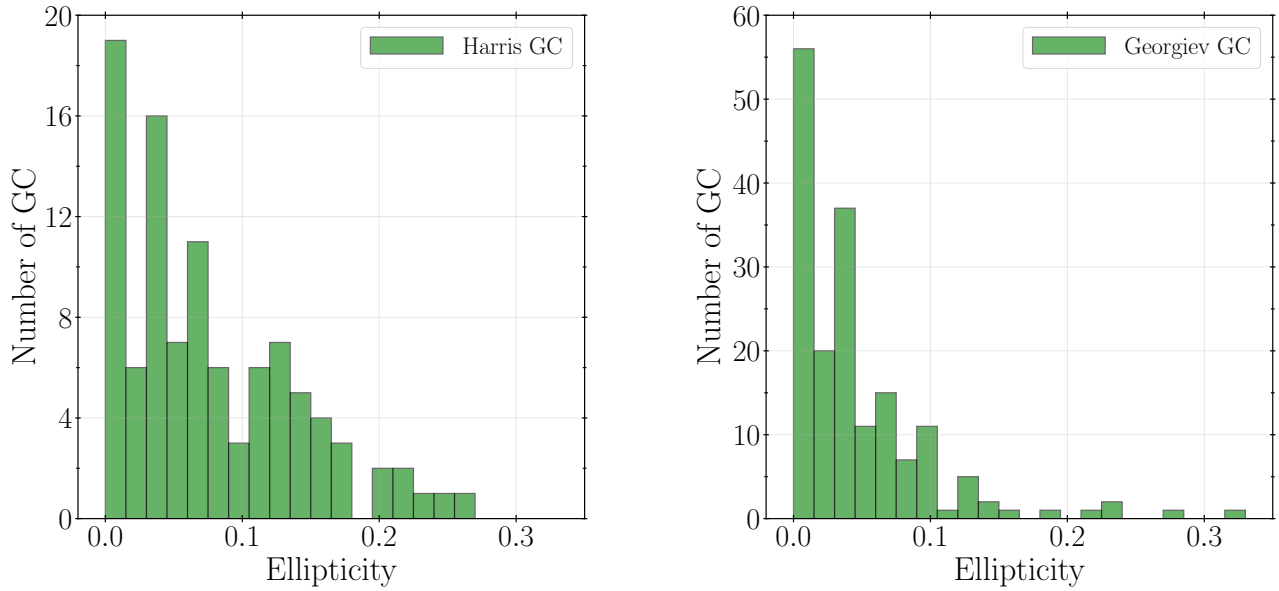

Figure 3.4: Ellipticity distribution of globular clusters in Harris (left) and Georgiev (right) data. 94% of the GCs lies between ellipticities of 0 and 0.2.

Is important to check if ellipticity has some relation with effective radius or with magnitude. To explore this, some plots have been done where ellipticity is shown against these two magnitudes. Figure 3.5 shows that there is no relationship between effective radius and ellipticity, nor between effective radius and magnitude. Although not shown here, we find the same results for the Georgiev catalogue.

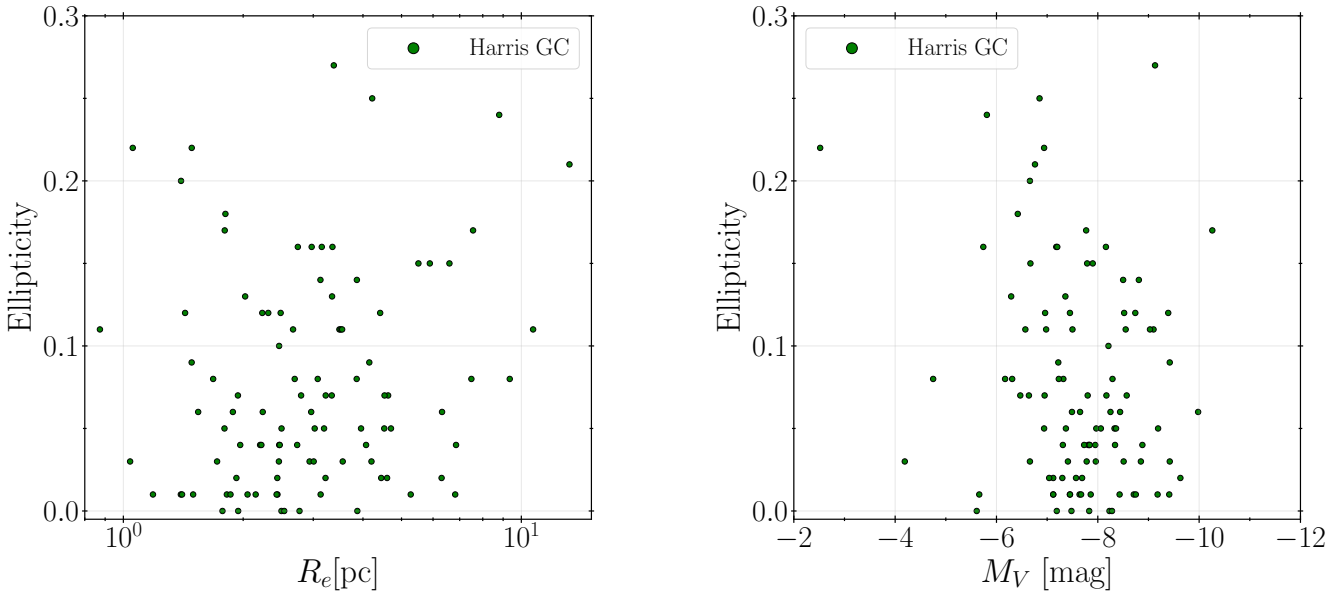

Figure 3.5: Ellipticity against effective radius (left) and ellipticity against absolute magnitude (right). Both of them for Harris' globular clusters. No obvious relations are found.

3.2 Data of MATLAS-2019

The data used in this work comes from two different set of observations carried out with the Hubble Space Telescope (HST). The first one are observations from the Advanced Camera for Surveys (ACS) and the second one from the Wide Field Camera 3 (WFC3).

3.2.1 Advanced Camera for Surveys imaging

MATLAS 2019 was observed by the HST using the WFC in the ACS instrument during the Mid-Cycle 27, program GO-16082 (PI: Müller). The data was obtained from the MAST archive [1]. The filters used in these observations were *F606W* ($\lambda_{\text{eff}} = 5809$ Å) and *F814W* ($\lambda_{\text{eff}} = 7973$ Å).

The galaxy is placed at the center of one of the CCDs, avoiding the gap between them. The images that are used are Charge Transfer Efficiency Corrected (CTE-corrected), *.drc.fits* images, produced by the standard pipeline of the instrument. These images are used because the HST has been in orbit for 33 years now and the cumulative effects of radiation result in a declining charge transfer efficiency.

The exposure time of the images is of 1030 seconds and its AB zeropoints used are 26.486 mag for *F606W* and 25.935 mag for *F814W*. These values are obtained from the ACS Zeropoint Calculator [2], introducing the date of the observations, which is 24/05/2020. The gain of the image is 2.0 e^-/ADU.

3.2.2 Wide Field Camera 3 imaging

MATLAS 2019 was also observed by the HST using the UVIS channel in the WFC3 instrument during the cycle 28, program GO-18284 (PI: Danieli). The data was also obtained from the MAST archive. The filters used were *F475W* ($\lambda_{\text{eff}} = 4731$ Å) and *F606W* ($\lambda_{\text{eff}} = 5780$ Å). Again, the galaxy is placed at the center of one of the CCDs. These images are also CTE-corrected, so we keep working with *.drc* images.

The images have an exposure time of 2349 seconds in *F475W* image and 2360 seconds in *F606W* image. The instrumental AB zeropoints are obtained as described in the WFC3 Data Handbook (9.1 Photometry)[3], using the `PHOTFLAM` and `PHOTPLAM` header keywords. The values obtained are 26.06 mag for *F606W* and 25.68 mag for *F475W*. The date of the observations was 2020-12-27. The gain of the image is 1.5 e^-/ADU.

3.3 Analysis tools

This study is carried out in the Python programming language. This choice has been made because Python, as any other high level programming language, provides a quickly way of working and manipulating the data of interest. Also, the extensive and valuable amount of data manipulation and astronomical libraries plays a central role (numpy, photutils, astropy...).

In addition, this work is also based on the tool called "SExtractor". SExtractor (Source Extractor) is a software that detects objects in astronomical images. The output catalogues provide different parameters of interest for the study to be carried out (mainly geometric and photometric parameters).

For representation and visual analysis of the data, the SAOImageDS9 software has been used.

3.4 Catalogue

In order to analyze the sources in the images and carry out the globular cluster study, the first step is to build a catalogue. This catalogue should contain the largest possible number of real sources and the less possible number of artefacts. This is not an easy task, since as we detect fainter sources, the amount of noise in our catalogue

[1] https://mast.stsci.edu/portal/Mashup/Clients/Mast/Portal.html
[2] https://www.stsci.edu/hst/instrumentation/acs/data-analysis/zeropoints
[3] https://hst-docs.stsci.edu/wfc3dhb

increases. Nevertheless, considering that we will later filter the sources using various parameters, we can prioritize maximizing the detection of sources over minimizing noise.

Building the catalog consist of several steps, these will be shown using as reference the *F606W*/WFC3 images (our deepest data), even though we perform the same process in all the images.

3.4.1 Background estimation

The first step in order to build a catalogue of sources consists in estimate the background. It is well known that one of the most important aspects of data is its reference value. This reference value is the value of the data where there is no signal and over which the noise fluctuates. In astronomy this value is tipically called "sky" value or "background" value.

The background value is a result of the contribution from different sources of different nature. These sources goes from instrumental (mainly bias, dark and flats) to astronomical (for example light from undetected objects or from fainter undetected regions of bright objects). It is very important to build and subtract an accurate estimation of the background because the more precisely the background is measured, the more accurate our measurements will be. In our particular case, as we are interested in the globular clusters of the galaxy (which are compact and bright sources) we need to include the diffuse light of the galaxy in our background estimation, because it is not of interest for this study.

The first thing that we need to do is to check how the background looks in our images. This way we can detect whether it has some notable features or whether there is something to pay special attention. Figure 3.6 shows an image with its visualization parameters optimized for checking the background. The image has been filtered with a smoothing kernel and an appropiate contrast and bias have been selected so the background can be clearly seen. It is obvious that our background signal is not uniform, with a strong diagonal gradient, so our estimation of the background has to take into account these space-variation features.

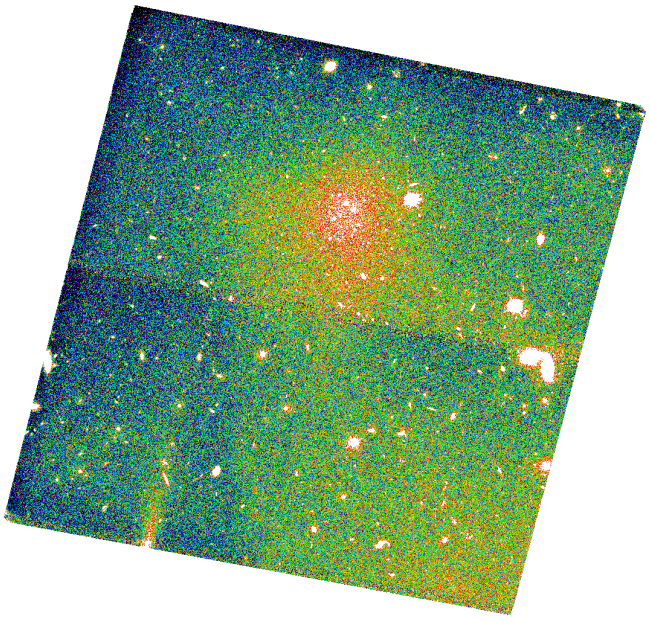

Figure 3.6: *F606W*/WFC3 image, smoothed to highlight the background variations. The galaxy MATLAS2019 is in the upper detector. Contrast and bias has been adjusted to show the background. The background is not uniform, with a notable diagonal gradient.

The background estimation is done with SExtractor, which shifts a square box through all the data, computing the mean and the standard deviation. This estimation is combined with a sigma-clipping and a mode estimation. After that, a median filter is applied to the background to suppress possible local overestimations.

There are two main parameters that we need to adjust in order to obtain our background. The first one is the size of the box that performs the first estimation (BACK_SIZE) and the second is the size of the median filter applied (BACK_FILTERSIZE).

The value of BACK_SIZE is really important. If we choose a value too small, compared to the objects to study, our background will include light from them and the estimation of their properties will not be accurate. However, if we choose a value too large we will not be able to reproduce small scale variations. The way of determining an appropriate BACK_SIZE is checking the average size of the objects that we want to measure.

Figure 3.7 shows a comparison between sources in the images and boxes of different sizes. It is clear that the smallest box (side of 32 pixels) is too small as it is similar to the size of the objects. Between a grid of 64 or 128 pixels it is not clear which one would be better, they are both quite reasonable although the 128 grid may seem somewhat large to detect small-scale variations.

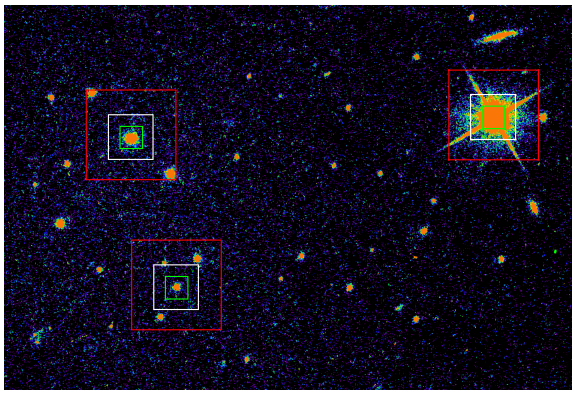

Figure 3.7: Comparison of different grid sizes with the size of the sources of the image. The size of the sides of the boxes are 32 (green), 64 (white) and 128 (red) pixels.

The other parameter, BACK_FILTERSIZE, is also important because the size of the median filter applied can vary significantly the background map that is obtained. The typical grid size for applying this filter is 3x3 pixels, although larger values are usually used to compensate small BACK_SIZE values.

Different background maps have been generated and compared in order to find the most suitable for this work. Grid sizes from 64 to 128 pixels and median filters from 1x1 (no median filter) to 6x6 sizes were tried. Background maps with BACK_SIZE of 32 and 256 were also generated to study the results obtained when using inappropriate parameters.

Figure 3.8 shows a comparison of the inner region of MATLAS-2019 after subtracting different background estimations obtained using different combinations of the values of BACK_SIZE and BACK_FILTERSIZE obtained from the previous analysis. This way, the over and under subtractions of the background estimation can be observed. It can be seen how a BACK_FILTERSIZE of 6 is too big and light from the diffuse body of the galaxy is still present, with a large grid (BACK_SIZE = 128) there is also some diffuse light from the galaxy left. This matches our previously study of the sources sizes.

To check the robustness of the chosen parameters, we have plotted the histogram of the detections employing different background parameters. This way we can see how the background parameters affects to the detection process of the sources.

In figure 3.9 the histograms obtained are shown, they correspond to the configurations shown in Figure 3.8. The detection threshold has been set to 1.1 (signals above 1.1 times the background RMS level will be catalogued as objects) so we can explore how the background affects the detection of faint sources, where the background plays a biggest rol. For now the photometry is done with the automatic mode of SExtractor. The shape of the histogram is similar regardless of the parameters used, indicating that the detection is quite robust with respect to the parameters as long as they are reasonable.

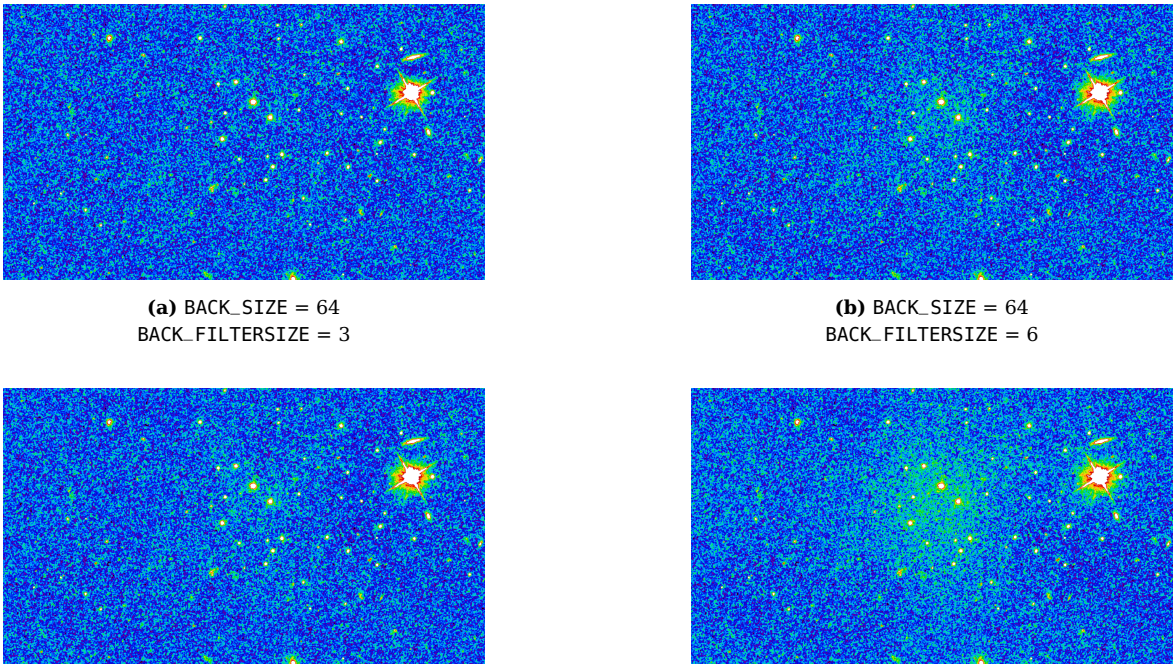

(a) BACK_SIZE = 64
BACK_FILTERSIZE = 3

(b) BACK_SIZE = 64
BACK_FILTERSIZE = 6

(c) BACK_SIZE = 128
BACK_FILTERSIZE = 3

(d) BACK_SIZE = 128
BACK_FILTERSIZE = 6

Figure 3.8: Smoothed center region of the galaxy MATLAS2019 with different background estimations subtracted. The scenarios with BACK_SIZE of 128 seems to not include all the galaxy light in the background estimation. The same happens when big median filters are applied. The set of parameters BACK_SIZE = 64 and BACK_FILTERSIZE = 3 produces the best results.

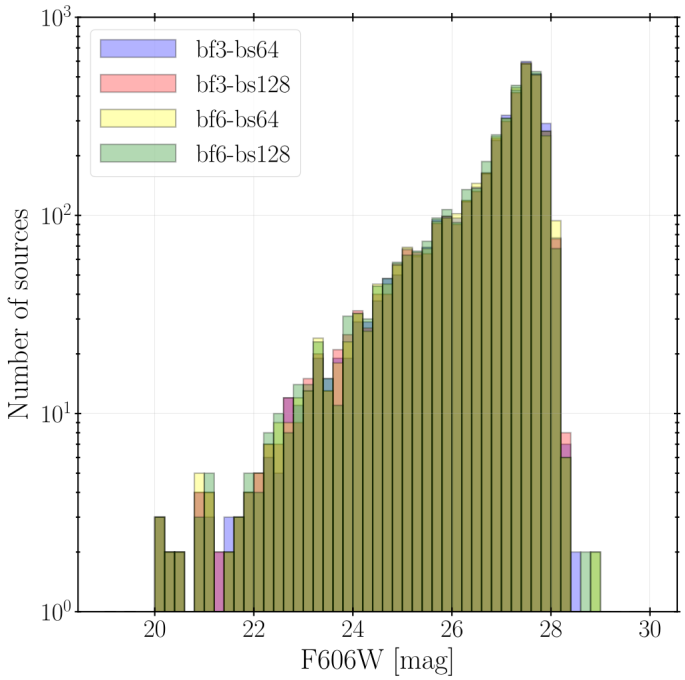

Figure 3.9: Comparison of the number of detected sources with respect the magnitude using different background parameters. The legend terminology attends to BACK_SIZE as bs and BACK_FILTERSIZE as bf. The shape of the histograms does not vary significantly.

After the study of the pixel size of the sources in the image, a visual inspection looking for under and over subtractions and the histograms of detections, we concluded that the best background estimation is obtained with `BACK_SIZE` = 64 and `BACK_FILTERSIZE` = 3. In figure 3.10 can be seen the final estimation.

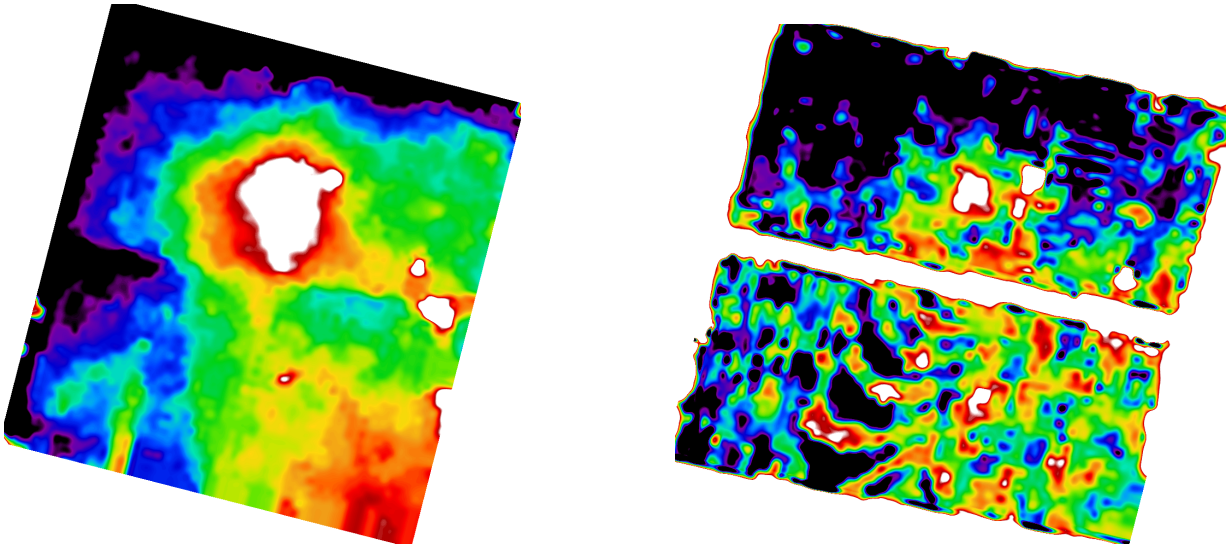

Figure 3.10: Left: Background map obtained using the best parameters found (`BACK_SIZE` = 64 and `BACK_FILTERSIZE` = 3). Right: Root Mean Square (RMS) of the background map.

To check that the background that we have subtracted is reasonable, the distribution of values in some signal free regions (regions without sources) of the background subtracted image is shown. After subtracting an accurate background estimation, we should find a Gaussian distribution centered in zero for the background pixels. In Figure 3.11 is shown that this is in fact the case, finding a Gaussian distribution centered approximately in zero with some amplitude given by the noise.

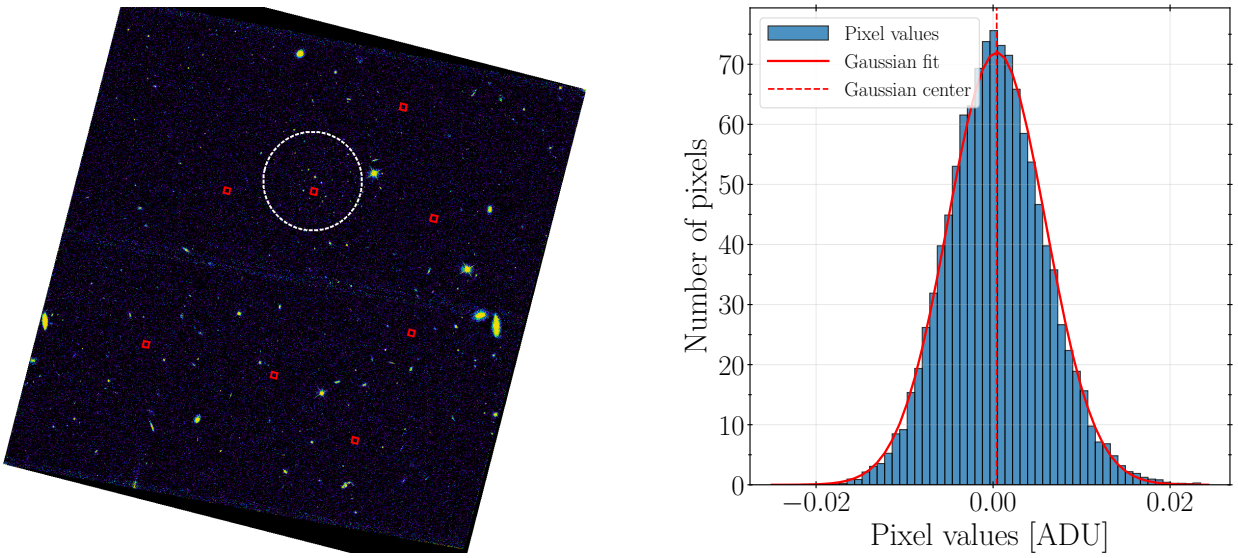

Figure 3.11: Left: Random regions (red squares) with no sources in which the values of the pixels have been evaluated. The size of the regions is 50x50 pixels. The dashed white circle indicates the location of the galaxy. Right: Distribution of pixel values in the previous regions. We find a Gaussian distribution centered approximately in zero ($\mu = 4 \times 10^{-4}$ ADU) with some width ($\sigma = 5.5 \times 10^{-3}$ ADU), resulting from the noise of the image.

3.4.2 Detection parameters

Once the background estimation is obtained, the next step is determine which detection parameters will be used for the creation of the catalogue.

SExtractor works with three detection parameters. The first one is `DETECT_THRESH`, and determines the threshold for detecting a pixel as part of an object. The second one is `ANALYSIS_THRESH`, a threshold used for determing a few output parameters (the only one of them that interests us is the measure of the FWHM). We will set these two thresholds to the same value. The third parameter is `DETECT_MINAREA`, which defines the minimum number of adjacent pixels exceeding the detection threshold to be considered a source.

There are three ways in which the thresholds can be specified: Surface brightness, ADUs and relative to background Root Mean Square (RMS). We will define the thresholds using the last way, relative to the RMS value. More specifically, the value selected is the number of RMS above the background for a pixel be detected as an object.

The values used for the thresholds varies considerably in the literature. Generally used values goes from 1.0 to 3.0 (e.g., Akhlaghi and Ichikawa 2015; Müller et al. 2021). As our catalogue of sources will be filtered later on by different constraints, we will to try to find all the possible sources that we are able to, this is, using a low value for the threshold (for example a value between 1.0 and 2.0).

About the minimum number of pixels needed for detection (`DETECT_MINAREA`), it is recommended in some SExtractor's manuals (Holwerda, 2005) to set it to a small value (from 1 to 5 pixels) and delegate the detection sensitivity to the threshold parameter (this is due to noise correlations, complex interplay of object topology and sampling). We will set it to 5, which is a small value but will reduce the probability to detect noise.

Knowing this, we have narrowed down the range of possible values for the thresholding. We have explored a number of values to see its effect on the detection of sources. As stated before, thresholds values between 1.0 and 2.0 are reasonable for our porposes, so we explore some of the values (1.1, 1.3, 1.5 and 1.8) within this range.

The easiest way to determine if we are using an adecuate threshold is by visual inspection. We compare our background subtracted image with the segmentation images obtained in the construction of the catalogue. Figure 3.12 shows this comparison for some feasible values.

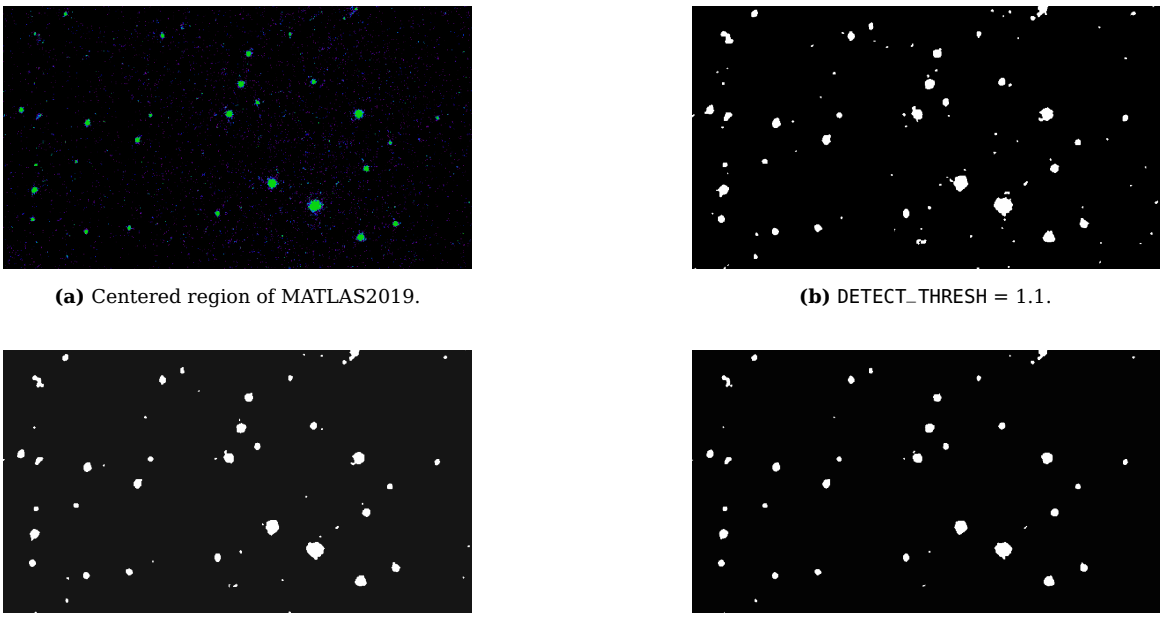

(a) Centered region of MATLAS2019.

(b) `DETECT_THRESH` = 1.1.

(c) `DETECT_THRESH` = 1.3.

(d) `DETECT_THRESH` = 1.5.

Figure 3.12: Comparison between the image of the galaxy (background subtracted) and some segmentation images obtained using different detection thresholds.

The number of detections decreases as the threshold value increases. When using a very low threshold like 1.1, a larger number of sources are detected. In fact, when we compare with the image some of them can not be seen, likely noise artefacts. With the highest threshold all the sources found with a first visual inspection are still detected, but when we check for very faint objects we start to miss some detections.

Therefore, from this visual inspection we can conclude that a threshold of 1.3 seems a good compromise between detecting spurious objects and trying to detect the faintest sources.

It is important to check how the detection histogram look like with the different thresholds. Figure 3.13 shows the comparison between the histograms obtained using different detection thresholds. The number of sources increases as the threshold decreases, but the important feature is the shape of the histogram. The number of sources observed as we go to fainter magnitudes increases exponentially. In a logarithm scale this looks like a straight line. This way, an adequate threshold value should provide us a histogram with this behaviour.

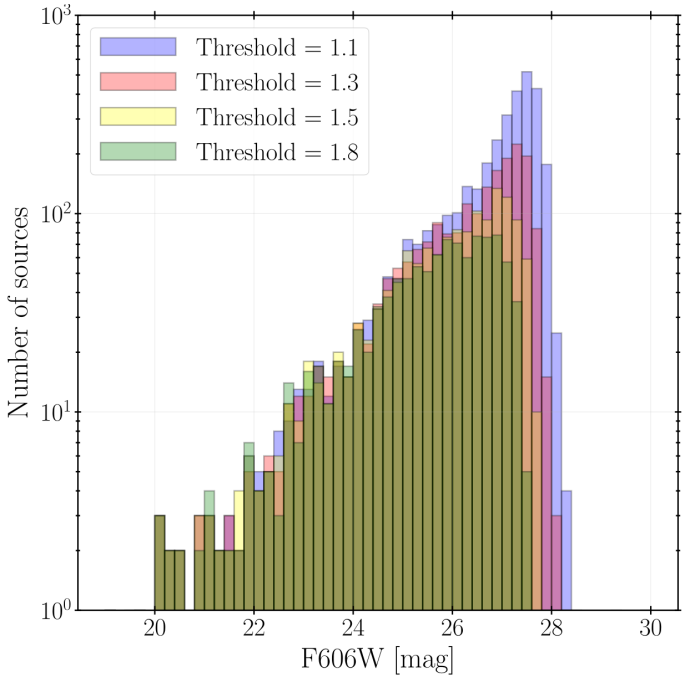

Figure 3.13: Comparison of the number of sources detected with respect the magnitude using different detection parameters. The shape of the histograms varies significantly, showing some of them growing too fast and others too slow with respect the expected exponential grow.

The increase in the number of sources have a exponential behaviour for low magnitudes (from 20 to 25) independently of the threshold parameter. However, from this point the different histograms start to show differences.

The higher detection threshold (1.5 and 1.8) lose their exponential behavior by stopping growing as fast as they should. This is interpreted as a deficiency in the detection of faint but real sources. The lower threshold (1.1) shows a better exponential shape but this time at the end too many sources are detected. This is the opposite problem and means that some noise is catalogued as real detections.

This way, the histogram obtained from the 1.3 threshold seems to be the one which behaves more like an exponential. This is consistent with the results obtained from the visual inspection, where this value also seems to provide the best detection results. For the above reasons, a threshold of 1.3 is used on what follows.

3.4.3 Deblending parameters

The next set of parameter are the deblending parameters. These parameters determine the way that is decided if a group of signal pixels are a single object or if there is more than one.

The field in which we are working is not crowded so the importance of the deblending is minor (regarding the other sets of parameters), albeit we should not forget about them as there can be situations where they can be relevant, like the alignment by chance of two sources. There are two parameters to explore: `DEBLEND_NTHRESH` and `DEBLEND_MINCONT`.

The first one defines the number of levels that SExtractor will create between the detection threshold and the maximum count of the detection. Based on these levels a tree of objects is built, branching when pixels above the threshold are separated by pixels below them. The second one defines the fraction of total counts (regarding the number of total counts of the detection) that a branch of the tree has to reach to be considered an individual object.

Based on some analysis of overlapping sources, is found that the default values provided by SExtractor documentation are good enough for our porpouses. These are `DEBLEND_NTHRESH` $= 32$ and `DEBLEND_MINCONT` $= 0.001$.

3.4.4 Photometry

Using the parameters studied so far, we can build a catalogue. However, we still need to explore how the photometry is performed. The photometry is dependant of two values of the input images, the gain and the zeropoint. These were provided in the data section. All magnitudes are given in the AB magnitude system.

SExtractor has multiple ways to perform photometry: *isophotal*, *isophotal-corrected*, *automatic*, *best estimate* and *aperture*. We use two: *automatic* and *aperture*. The reason why we use these modes is that the *isophotal* mode is too simple (uses the detection threshold as the lowest isophote) and the *isophotal-corrected* and *best estimate* are deprecated (they remain in current SExtractor versions for compatibility). They are also the most widely used, which allows a better comparison with photometry from other authors.

Automatic mode

The automatic photometry mode of SExtractor (`MAG_AUTO`) uses an adaptively scaled aperture called `KRON_RADIUS` for every source. This aperture is based on the Kron's "first moment" algorithm and theoretically encloses 90% of the object's light, allowing SExtractor to calculate an optimum aperture for each detected object.

There are also some possibilities for tuning this photometry, like defining a scaling parameter for this Kron radius (this allows you to include more flux with the penalty, of including more noise) and defining a minimum possible aperture for performing the measurements. In any case, the default parameters work fine for almost every situation so we will work with them.

Figure 3.14 shows the `MAG_AUTO` histogram of the *F606W*/WFC3 image. The number of sources increases towards faint magnitudes following a exponential growth. The peak is found around 27 magnitudes, which is around limiting magnitude that we can detect. At fainter magnitudes there are some detections, probably noise.

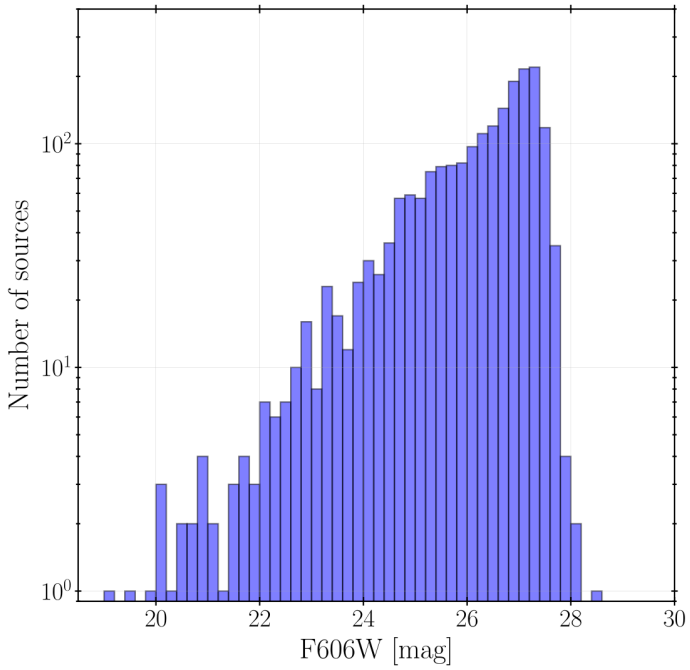

Figure 3.14: Number of sources detected with respect the magnitude using `MAG_AUTO`. Up to 27 magnitudes we find a exponential growth in the number of sources.

Aperture mode

The aperture mode is one of the typical and most used ways of performing photometry. In aperture photometry, we have to define an aperture size and the photometry is performed based on the flux which falls into this aperture.

This way, the important thing that we have to define is the radius of the aperture that we are going to use. An aperture of two times the Full Width Half Maximum (FWHM) of the PSF (which is a measure of the extension of a point-like source in the image) is typically used because it encloses more than 99% of the light (assuming a Gaussian light profile). This is perfectly fine when you are looking for point-like sources, but we are looking for globular clusters. Do globular clusters appear like point sources in our data?

The distance to MATLAS-2019 is not yet agreed, values of 21 Mpc and 26 Mpc are found with different methods. In this situation the study has been done exploring both distances. This way, knowing the distance at which the galaxy is (21 or 26 Mpc) and the angular resolution of our instrument (0.04 arcsec/pixel for WFC3 and 0.05 arcsec/pixel for ACS) is enough to determine the typical size for a GC in our images.

In fact, the parsecs covered by one single pixel for the different distances and instruments vary from 4 to 6 parsecs. From our previous study of reference globular cluster (Harris' and Georgiev's globular clusters) we know that globular cluster typical effective radius is around 3 or 4 parsecs. Based on these two values, we are able to resolve or partially resolve the GCs of this galaxy. Therefore an aperture based on point-like sources would not be adequate as we might miss flux doing so. In order to estimate the optimal aperture for the GCs, we will need to estimate the FWHM that they have in the images.

The apparent size that a source have in an image is a product of the convolution of the source's light profile and the PSF. For doing this convolution, we assume that the GC profile can be approximated with a Gaussian. We will assume the same for the PSF. This way can convolve them analytically using their standard deviations like it is shown in equation 3.1.

$$\sigma^2_{\mathrm{convolved}} = \sigma^2_{\mathrm{a}} + \sigma^2_{\mathrm{b}} \tag{3.1}$$

The PSF of the HST images on the different filters are empirical models provided by the Space Telescope Science Institute (STScI[4]). The PSF of *F606W*/WFC3 image will be used for illustranting the process, Figure 3.15 shows this empirical PSF.

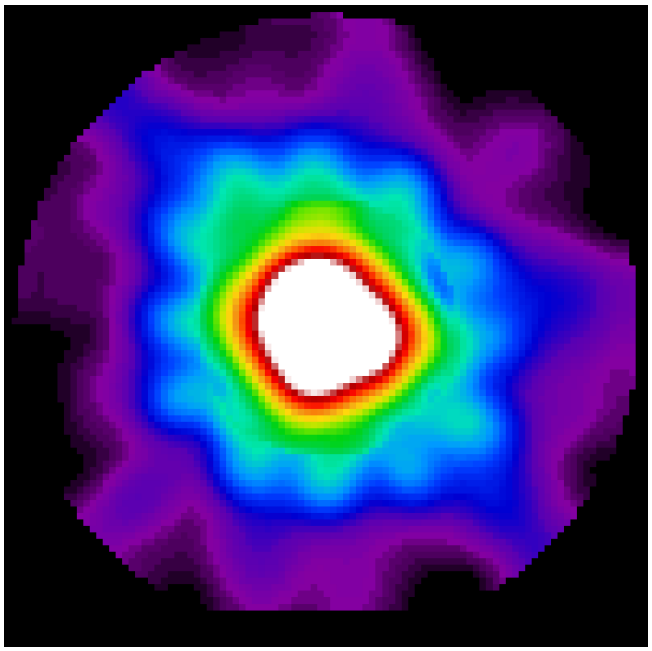

Figure 3.15: Empirical PSF of images on the filter *F606W* for the WFC3 instrument.

Once we have the PSF empirical model, a Gaussian fit is performed to the PSF. Figure 3.16 shows a 3D view of the Gaussian fit performed. Additionally, in figure 3.17, a 2D projection of the original and fitted profiles is also shown (the PSF is oversampled by a factor of 4).

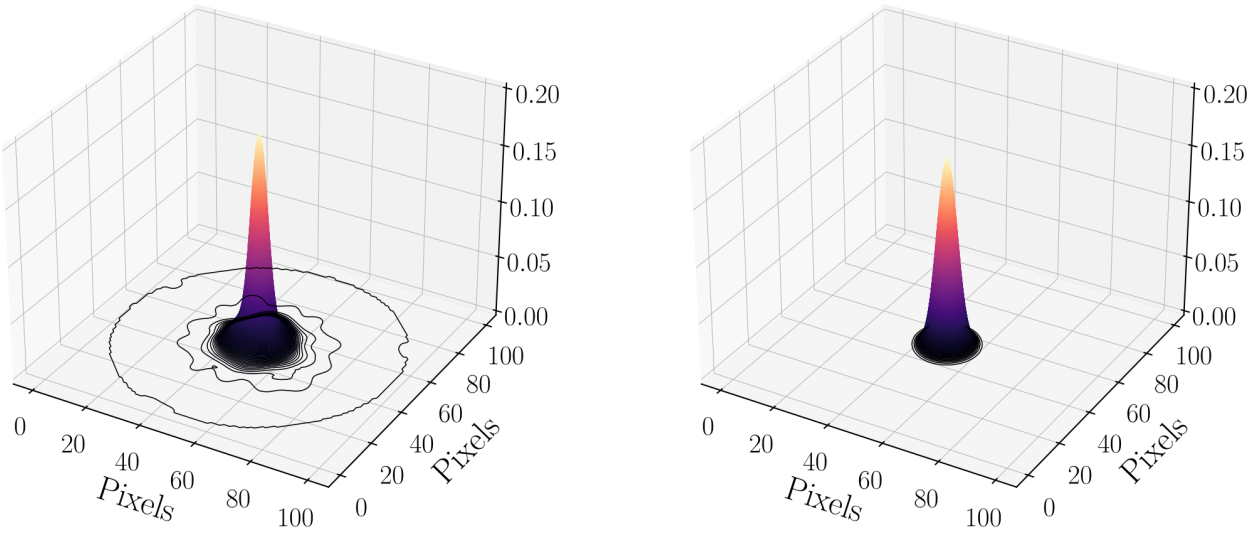

Figure 3.16: Left: 3D view of the empirical PSF model of WFC3 instrument in the filter *F606W*. Right: 3D view of the Gaussian fit of the previous PSF empirical model. The model is oversampled by a factor of 4 because this is the sampling in which the STScI provides the PSF.

[4]https://www.stsci.edu/hst/instrumentation/wfc3/data-analysis/psf

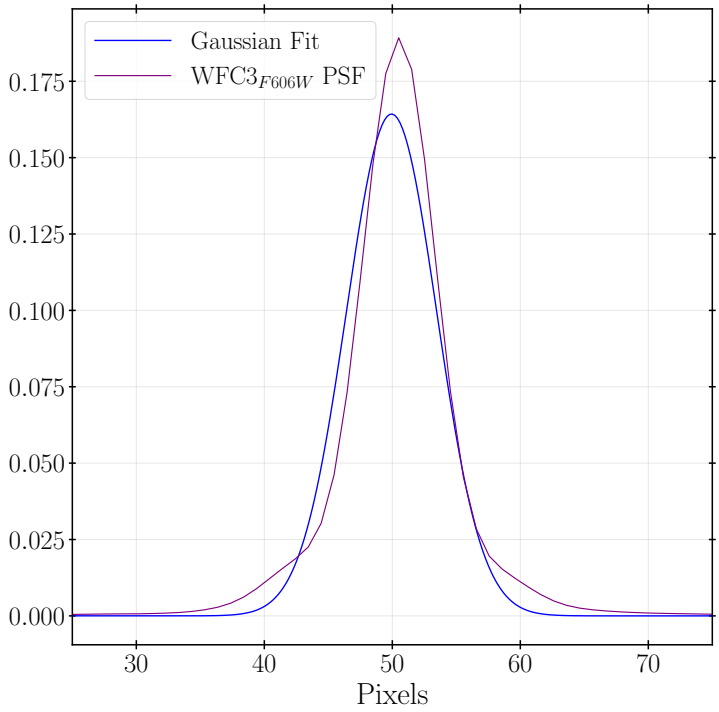

Figure 3.17: 2D projection comparison of the PSF empirical model and its gaussian fit. The model is oversampled by a factor of 4.

The Gaussian fit obtained is reasonable and enough for our purposes of characterizing σ. The Gaussian has a slightly different standard deviation in the two axis but the difference is not big (0.09 pixels after undersampling to the real size). This way, as an aproximation, a constant standard deviation will be assumed by averaging both values. The final σ (after undersampling) that will be used is 0.86 pixels (0.034 arcsec).

After fitting the PSF we need to characterize a (typical) globular cluster. In the analysis performed in Section 3.1 it was found that a typical globular cluster has an effective radius around 3.6 pc. Assuming a gaussian profile for the source, we convert this effective radius to standard deviation applying the analytical relation $\sigma = \sqrt{\frac{R_e^2}{2\ln(2)}}$.

This way a standard deviation of 3.057 pc is obtained. This value is converted to pixel units by a parsec to pixel factor that is easily calculated knowning the distance to the galaxy. For example, assuming that the galaxy is at 21 Mpc with a resolution of 0.04 arcsec/pixel (WFC3), the σ value for the globular cluster would be 0.76 px.

Given that the standard deviation of the PSF and that of a typical GC are similar, we have to take into account both profiles. Convolving these two Gaussian profiles using the expression 3.1, we obtain an observed standard deviation of 4.60 pc or 1.15 px. This new profile represents a typical globular cluster in our image. Figure 3.18 shows a comparison of the two profiles (PSF and GC using Gaussian approximations) and the convolved profile assuming a distance of 21 Mpc.

At this point we are ready to determine the aperture that will be used in the photometry. Transforming the standard deviation to FWHM by applying the analytical relation FWHM = $2\sigma\sqrt{2ln(2)}$, we obtain a value of 2.70 px (distance of 21 Mpc). This means that when we define the aperture as two times the FWHM, an aperture of around 5 pixels of radius is reasonable.

Doing an analog process assuming a distance of 26 Mpc, the value obtained for the FWHM is 2.48 px. When we apply the criteria, we find that an aperture of 5 pixels is also adequate.

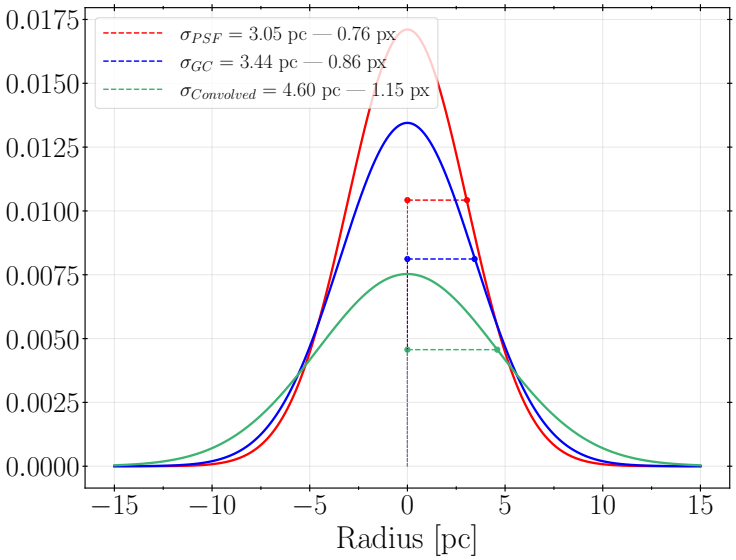

Figure 3.18: 2D comparison of the Gaussian approximation of the PSF, the Gaussian approximation of a typical globular cluster and the profile obtained from convolving these two. A distance of 21 Mpc is assumed for the conversion to physical units. The horizontal lines respresent the standard deviation of each profile.

The number of sources obtained from performing photometry with this globular cluster oriented aperture is shown in figure 3.19. The shape is still exponential, although we have to keep in mind that since we are using a specific aperture for globular clusters, this will not produce an adequate photometry for other type of sources.

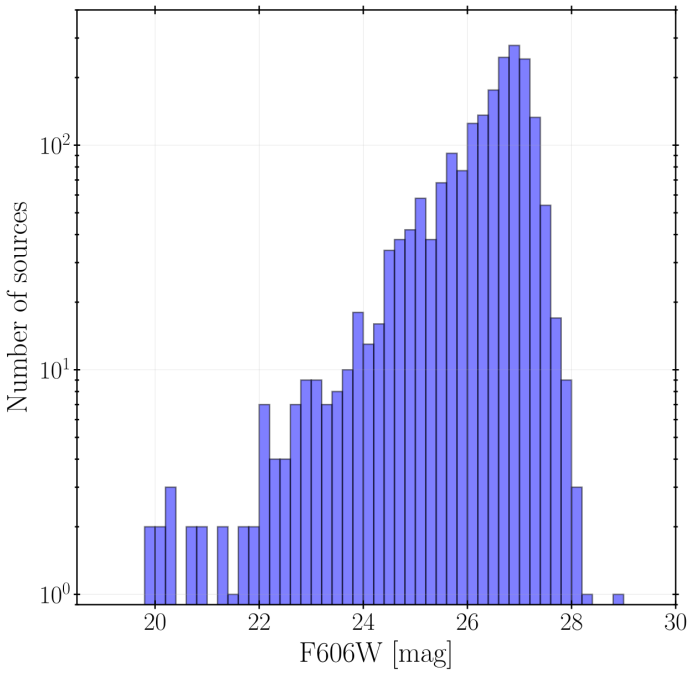

Figure 3.19: Number of sources detected with respect the magnitude using aperture SExtractor's mode with an aperture calculated based on the PSF and a typical globular cluster size.

A comparison between the two photometries performed (automatic and aperture) is shown in Appendix A.

Photometric corrections

There are two important corrections to be made to the photometry: Encircled energy (EE) and Galactic extinction. Both of them will be applied to our aperture photometry but, since the automatic photometry adjusts the aperture to the source size and captures almost all of the object's light, this will only be corrected from extinction.

The encircled energy correction (correction to infinite apertures) is a correction realized to take into account the flux that is lost due to the use of a finite aperture. Strictly speaking, this is a point source correction but since our sources are not too extended (the GCs are only partially resolved with a difference of around 0.4 px between the PSF profile standard deviation and our GC model standard deviation) we will perform this correction to our aperture photometry as an approximation. The STScI provides the needed EE tables for performing the photometry corrections [5].

The extinction correction is a basic correction and of necessary application in any photometric measurement. The extinction coefficient for the different filters have been obtained from the NED Extinction Calculator [6] and are the following:

- *F475W* = 0.171 mag
- *F606W* = 0.131 mag
- *F814W* = 0.081 mag

These quantities are the extinction in magnitudes, so they are just subtracted from the photometric measurements obtained.

The magnitudes corrected of both effects (aperture photometry) differ from original magnitudes in 0.2-0.35 magnitudes as a function of the image (redder images are less affected by extinction).

3.4.5 Matching catalogues

At this point, we have a catalogue for each of the images that we have available, this is a *F475W* and *F606W* for WFC3 instrument and a *F606W* and *F814W* for ACS instrument.

The next thing that we have to do is to combine and match all these catalogues into a common one, which will be the one used for filtering and obtain the GC candidates. First of all it is necessary to decide which catalog (image) we will be used as the main one, to match the others to this one.

Main image analysis

The main criteria that will be used to decide which image is used as the main one is their depth. For this, we will characterize the typical flux measured in our globular cluster aperture in regions of the image where no sources are present. This is, characterizing the noise of the image.

In order to characterize this flux, a large number of apertures (20000) have been placed throughout the image and its flux has been measured. Previous to that, we masked all the sources of the image using a SExtractor's segmentation image and a manual mask for the galaxy, making sure that we strictly measure noise and not signal. In figure 3.20 is shown the mask for *F606W*/WFC3 image.

[5] https://www.stsci.edu/hst/instrumentation/wfc3/data-analysis/photometric-calibration/uvis-encircled-energy
[6] https://ned.ipac.caltech.edu/extinction$_calculator$

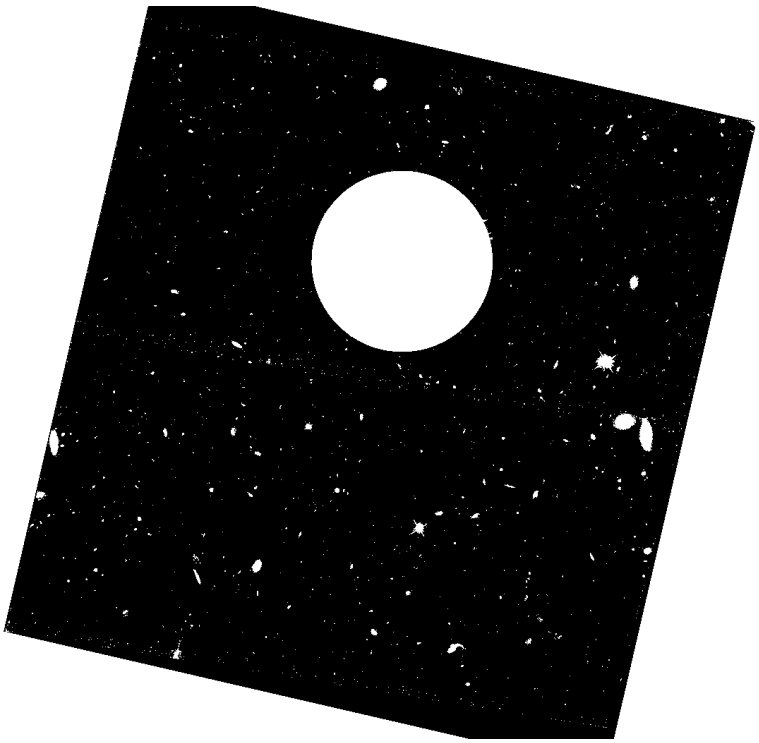

Figure 3.20: Mask applied to *F606W*/WFC3 image in order to characterize the noise.

In Figure 3.21 the distribution of fluxes in GC-like apertures can seen. The noise has a Gaussian shape and applying a gaussian fit, the 5σ distance is calculated. We use this 5σ value as numerical measurement of the flux value from which we (almost certainly) detect real signal, this is, the depth of the image.

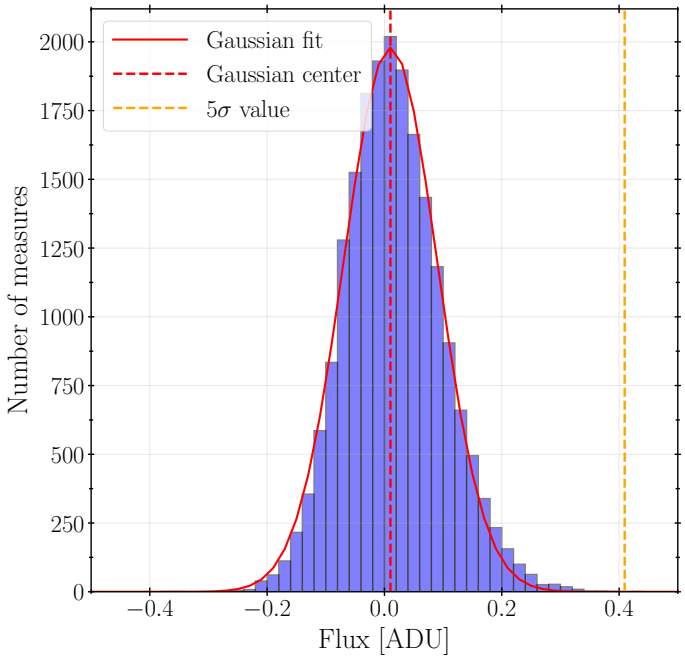

Figure 3.21: Flux within GC like apertures in regions placed randomly throughout the *F606W*/WFC3 background subtracted image. In red, a gaussian has been fitted and the 5σ value (yellow) has been calculated.

Doing this characterization for all the images the following depth limits are obtained:

- WFC3 - *F475W*: 26.91 mag
- WFC3 - *F606W*: 27.03 mag
- ACS - *F606W*: 26.86 mag
- ACS - *F814W*: 26.41 mag

This way, the *F606W*/WFC3 is the deepest image. This is the one that will be used as the main image for catalogue matching and individual image measurements (effective radius and ellipticity).

Matching

Once all the catalogues have been obtained (one catalogue per image) it is the moment to put them together. The catalogues which will be used are from filters *F475W*, *F606W* and *F814W*. As we have two images for *F606W* filter we will use the deepest, this is, the catalogue from the WFC3 camera.

An important point is that the field of view in WFC3 images and in ACS images is not the same. This way, the resulting catalogue will belong only to a section of the images (the common section between them). Figure 3.22 shows at the same time the field of view of the WFC3 and ACS images.

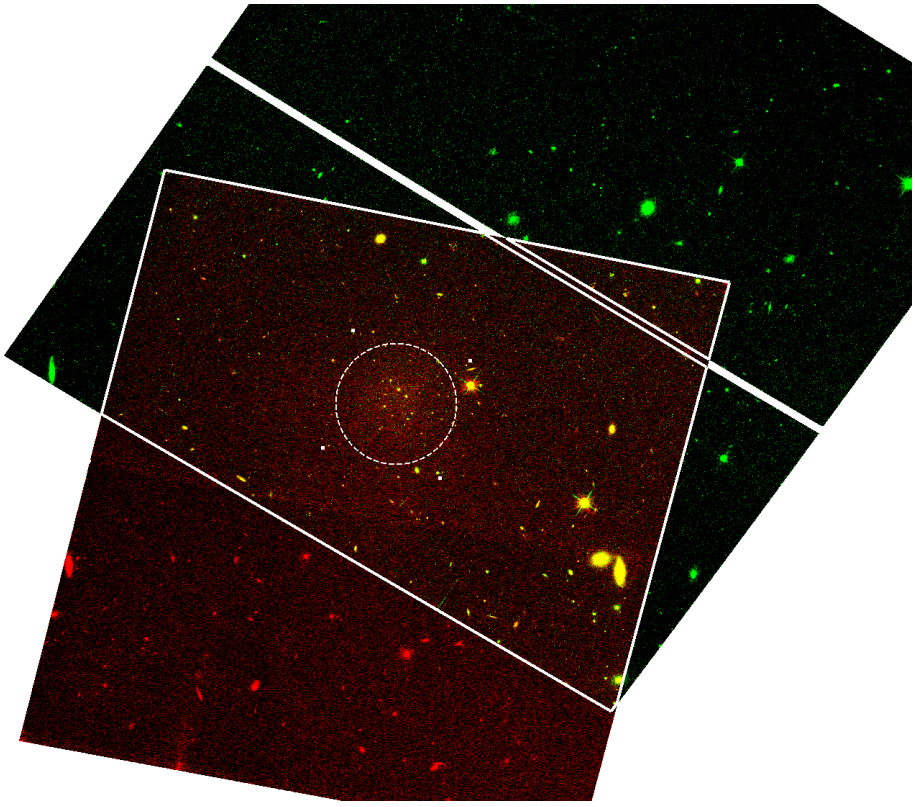

Figure 3.22: WFC3 image field of view in comparison with ACS image field of view. The common region (solid line) and the galaxy (dashed circle) are indicated in white. The final catalogue will have information of this common region.

The catalogue matching has been done with a tolerance of 0.5 arcsec. The final catalogue is shown in figure 3.23 with a total number of sources of 442.

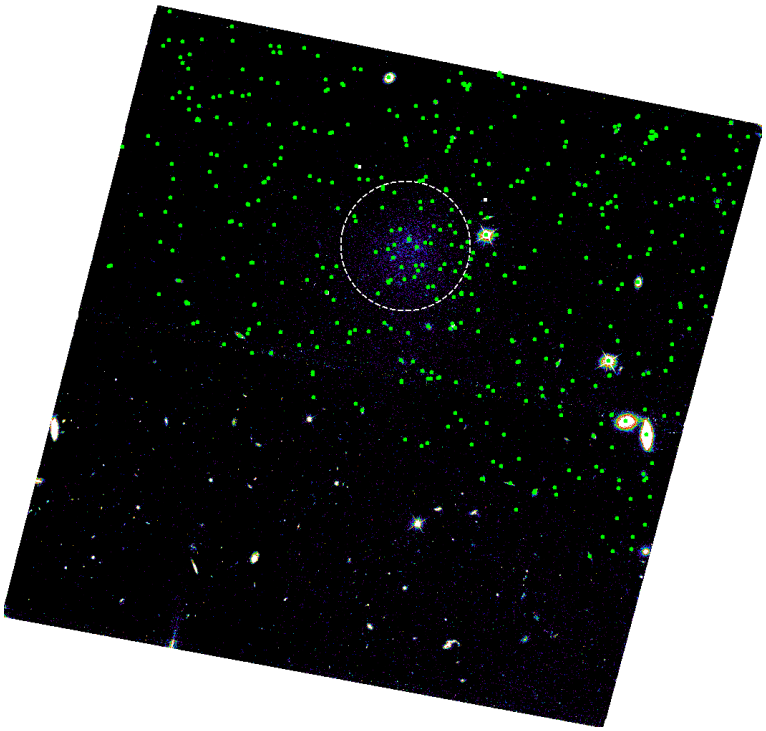

Figure 3.23: Position of the objects (green dots) obtained after merging the different catalogues of the different images. The white dashed circle indicates the location of the galaxy. Image from WFC3 filter *F606W*, smoothed.

3.5 Globular cluster selection

The next step is to filter the catalogue to obtain a clean sample of GCs. To select our globular cluster candidates, different criteria of magnitude, effective radius, ellipticity and colours will be used.

First, we filter by effective radius, ellipticity and magnitude. This is because these parameters are directly obtained from our reference *F606W* image. After this initial selection, a colour filtering is applied, in which all the catalogues are combined in order to get the colours.

3.5.1 Effective radius, ellipticity and magnitude

The ranges of values of effective radius, ellipticity and magnitude used in this study to select the GCs were obtained by combining information from two different sources: the confirmed spectroscopic globular clusters of MATLAS-2019 and the analysis of known globular clusters presented in section 3.1.

First, the analysis of the effective radius, ellipticity and magnitudes of the 11 spectroscopically confirmed globular clusters is presented. We analyze their range of values and, after this, all the information available about the parameters will be taken into account in order to define the ranges that will be used to filter the catalogue.

In figure 3.24, the effective radius, ellipticity and magnitude distributions are shown, usign for the magnitude measurements the SExtractor's `MAG_AUTO`. The same information is represented in figure 3.25 using the aperture calculated for globular clusters. These values are obtained from the *F606W*/WFC3 image assuming a distance of 21 Mpc (for the effective radius). In Appendix B.1 it can be seen the same figures assuming a distance of 26Mpc.

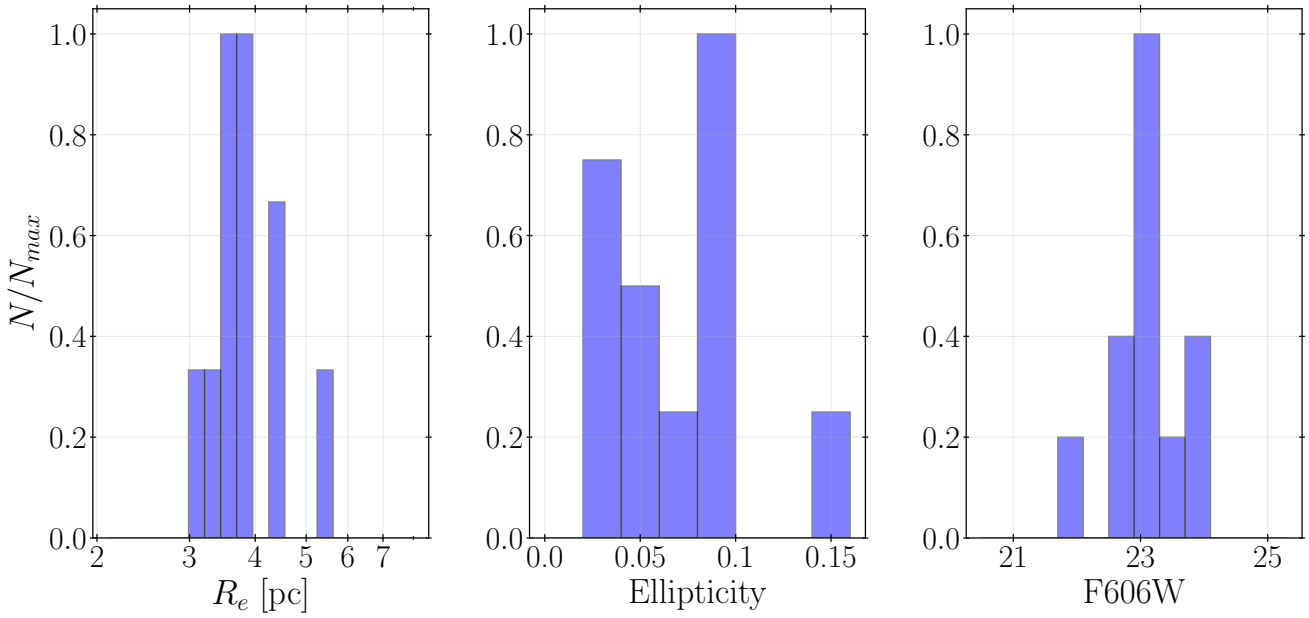

Figure 3.24: Effective radius, ellipticity and magnitude distributions for the spectroscopically confirmed globular clusters using SExtractor's `MAG_AUTO`. The distance assumed for the effective radius is 21 Mpc.

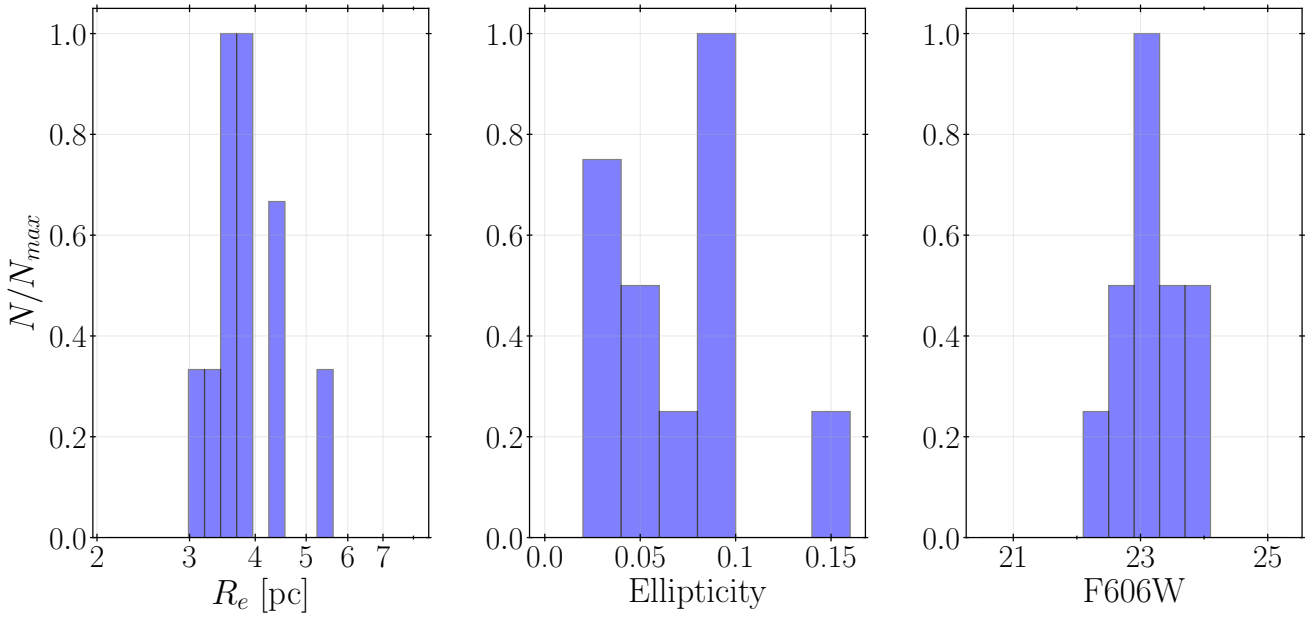

Figure 3.25: Effective radius, ellipticity and magnitude distributions of the spectroscopically confirmed globular clusters using aperture photometry. The distance assumed for the effective radius is 21 Mpc.

Effective radius

The first parameter that we are going to deal with is effective radius. The measured R_e is dependent on the distance, adding a layer of complication to the criteria that we are trying to obtain. Figure 3.24 shows that the effective radius of the spectroscopically confirmed GCs are distributed between 3 and 6 pc (between 4 and 7 at 26 Mpc). These are their intrinsic physical values, this is, deconvolved from the image PSF values.

The values (independently of the distance assumed) are consistent with the values seen in the anaysis of the Harris' and Georgiev's catalogues (Section 3.1.2), where almost all of the measurements of GC effective radius where below 10 pc. As all the spectroscopically confirmed GC are well within this range, this criteria is used.

Therefore, the maximum effective radius allowed for a source to become a GC candidate is 10 parsec (around 0.1 arcsec). No lower limit is set. We could use the size of the PSF, because in theory no source will be smaller than this (even if it is a point like source), but to reduce possible measurement errors of SExtractor (specially at faint magnitudes) we do not set a lower limit.

Ellipticity

The ellipticity that is found when analyzing the confirmed globular clusters goes from around 0.00 to 0.15. Even though theoretically GCs would be perfectly round, when measuring them typically we will find a deviation from this expected value.

Comparing these values with the ones from Harris and Georgiev (Figure 3.4) we find that they agree. In these datasets 94% of the GCs have ellipticities below 0.20, which is a slightly higher value that the higher value found in our confirmed GCs.

Setting the upper limit a little bit higher than the less elliptical confirmed GC is reasonable, taken into account for sources that might have been missing from the spectroscopic sample, as we have only 11 confirmed GC. This way, an ellipticity range from 0.00 to 0.20 is applied.

Magnitude

Next, the range of magnitudes that we will allow in our selection will be decided. In figure 3.24 and 3.25 the apparent magnitudes of the confirmed GCs are between 21.5 and 24 magnitudes. In this case, the magnitudes are a result of the depth reached by the spectroscopic study realized.

The magnitude distribution of the confirmed GCs that is found in the histograms is probably just the bright part of the GCLF. So we will also use another way to help us decide how to filter by magnitude. This is done by knowing the peak and typical width of the GCLF. The distribution of all the sources detected is plotted against the distribution that the GCLF should have, this way we can see in which range of magnitudes we should make the selection and if we are complete or not.

The GCLF has been characterized by peaking at $M_V = -7.6$ and with a $\sigma = 1.2$ (Rejkuba, 2012). In order to compare it with our detections we need to know how this distribution looks like in our image. For this we need to transform the absolute peaking magnitude in the *V* band (M_V) to an apparent magnitude in *F606W*.

The conversion is done using the distance modulus, which takes a value of 31.61 for 21 Mpc and 32.07 for 26 Mpc. Applying this, the GCLF should peak at $m_V = 24.01$ (21 Mpc) or at $m_V = 24.47$ (26 Mpc). What is left is transforming these quantities from the *V* band to *F606W* values. For the color of a typical GC, the relation is estimated to be $V - F606W = 0.13$ mag (Peng and Lim, 2016). Applying this we find that our GCLF is expected to peak at $F606W = 23.88$ for 21 Mpc and at $F606W = 24.34$ for 26 Mpc.

In figure 3.26 the magnitude distribution of the detected sources (blue) using `MAG_AUTO` is compared with the distribution that the GCLF should have (yellow Gaussian distribution). The left plot shows the comparison assuming 21 Mpc and the right one assuming 26 Mpc. The 2σ and 3σ regions are indicated in yellow and red respectively.

We can see that, independently of the distance, the magnitude distribution of the GCLF is basically within the complete range, with a 2σ level well included in our detection range. This means that we expect to recover most of the GCs of this galaxy. Of course, assuming 26 Mpc the faint tail of the Gaussian falls a little further than our detection limit, but the completeness correction, if needed, is small.

Regarding the range to filter the magnitudes of the GC candidates, it seems reasonable to accept arbitrarily bright sources. Most of these should have been already detected in the spectroscopic observation, but bright sources may exist outside the studied field (the MUSE FOV is 1 arcmin in Müller et al. (2021), considerably smaller than the WFC3 or ACS FOV). For the fainter limit it is also adequate to not define any threshold either, we are almost complete but there may still be candidates at our detection limit that we do not want to lose.

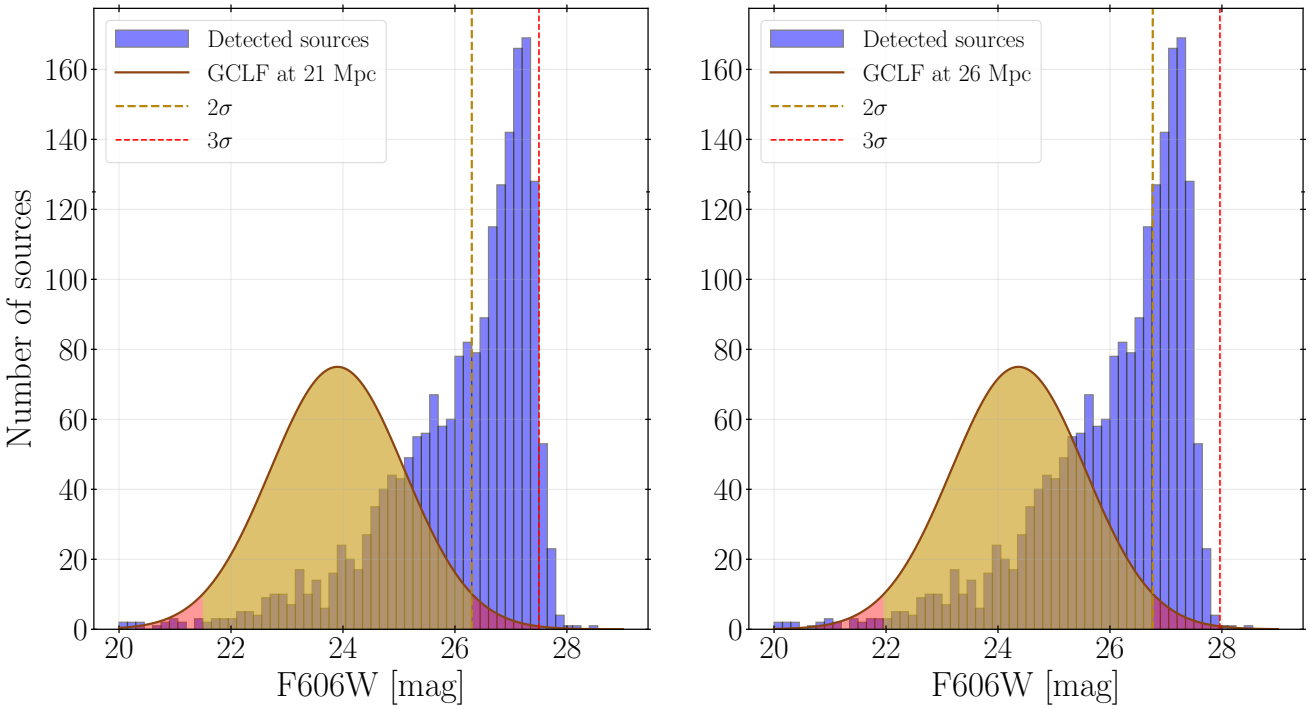

Figure 3.26: Magnitude distribution of the sources for *F606W*/WFC3 using `MAG_AUTO` (blue) compared with the expected GCLF (yellow Gaussian distribution; 21Mpc left and 26 Mpc right). The yellow area is a region of 2σ and the red tales complete the 3σ. It can be seen how the detection limit is reached somewhere between 2σ and 3σ.

Selection criteria of GC candidates summary

Before proceeding with the colour criteria a brief summary of the last sections is shown. The criteria that is applied to the effective radius, ellipticity and magnitude parameters are the following:

- Effective radius: [0.0, 10.0] pc.
- Ellipticity: [0.0, 0.20].
- All magnitudes allowed.

3.5.2 Colours

After performing the first selection by effective radius, ellipticity and magnitude, the colours of the objects are taken into account. Identifying GCs by their colors is a common strategy, due to the relatively limited colour dispersions that they show. Since we have 3 different bands, we can obtain two different colours. This way, we can construct a colour-colour diagram in which we expect globular clusters to be located in a well-defined range (Taylor et al., 2017).

To determine the colour ranges for the GC candidates selection, the location of the confirmed globular clusters in the diagram will be studied. In Figure 3.27 and 3.28 the colour-colour diagram (automatic and aperture photometry, respectively) is shown.

The colour ranges for accepting a source as a globular cluster are calculated from the median and standard deviation of the colours of the confirmed ones. This way, the standard deviations (σ) of the colours of the confirmed GC are computed and $\pm 3\sigma$ from the median is taken as the colour range. This colour region represents the colours of the confirmed GC taking errors into account.

This way, the colour ranges to apply are the following (first row of ranges for automatic photometry, second row for aperture photometry):

- *F475W* - *F606W* (Auto): [0.31, 0.60] mag
- *F606W* - *F814W* (Auto): [0.29, 0.49] mag
- *F475W* - *F606W* (Aper): [0.35, 0.56] mag
- *F606W* - *F814W* (Aper): [0.30, 0.50] mag

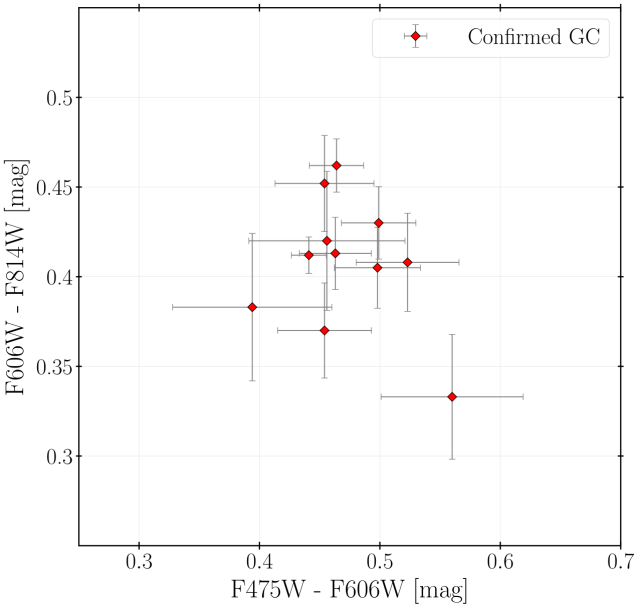

Figure 3.27: Colour-colour diagram using SExtractor's automatic photometry. The location of the confirmed spectroscopically globular clusters are shown.

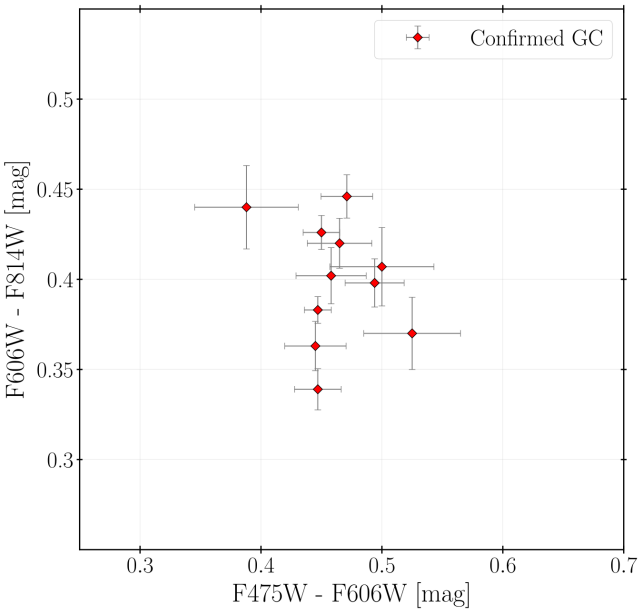

Figure 3.28: Colour-colour diagram using SExtractor's aperture photometry. The confirmed spectroscopically globular clusters are shown.

Chapter 4

Results

4.1 Effective radius, ellipticity and magnitude selection

We initially have a total of 442 sources detected and matched through all the images. After applying the effective radius, ellipticity and magnitude criteria decided in Sec. 3.5.1, a total of 134 sources remain.

The distributions of effective radius, ellipticity and magnitude of these sources are shown in the histograms of Figures 4.1 and 4.2 for automatic and aperture photometry respectively. The red histograms are the spectroscopically confirmed GC, the blue histograms are the objects which simultaneously satisfy all the criteria and the grey histograms are all the sources of the catalogue. The vertical black lines show the selection criteria of Sec. 3.5.1. The distributions are based on data from WFC3 instrument *F606W* filter assuming a distance of 21 Mpc. In Appendix B.2 we show the same figures assuming 26 Mpc.

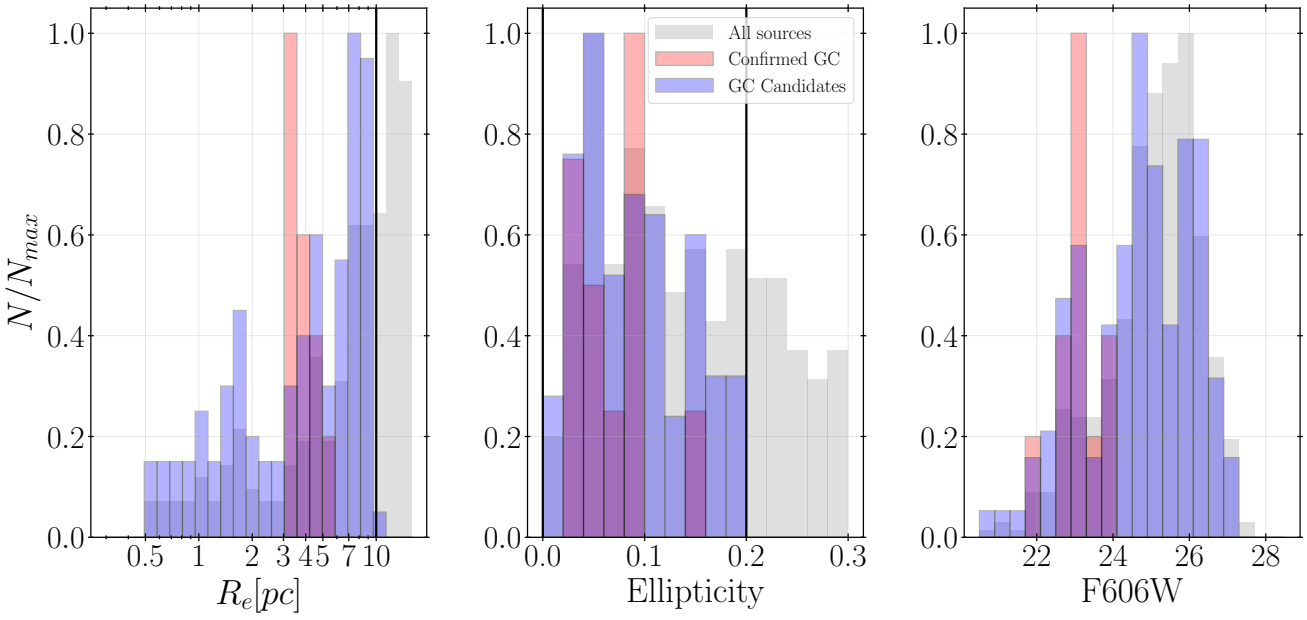

Figure 4.1: Effective radius, ellipticity and magnitude (automatic photometry) distributions of differente samples of sources. In red the GCs spectroscopically confirmed (11 sources), in blue the sources which fulfill all the conditions (134 sources) and in gray all the sources of the catalogue (442 sources). The vertical black lines are the ranges imposed in the GC selection. The assumed distance is 21 Mpc.

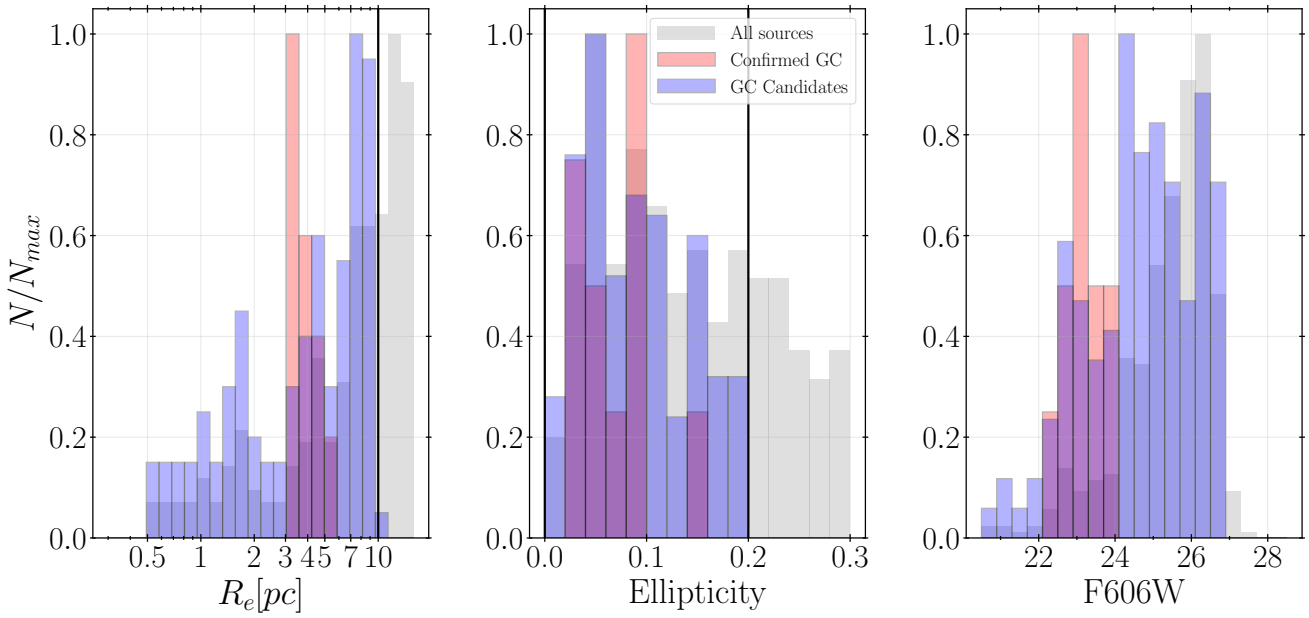

Figure 4.2: Effective radius, ellipticity and magnitude (aperture photometry) distributions of differente samples of sources. In red the GCs spectroscopically confirmed (11 sources), in blue the GC sources which fulfill all the conditions (134 sources) and in gray all the sources of the catalogue (442 sources). The vertical black lines are the ranges imposed in the GC selection. The assumed distance is 21 Mpc.

It is also important to check how the candidates distribute in the image. Figure 4.3 shows the *F606W*/WFC3 image with the selected objects at for 21 Mpc (Appendix B.3 for 26 Mpc). These candidates are found independently of the photometry mode used. As mentioned before, the catalogue only covers the common field between the cameras. The preliminary selected objects are spatially distributed quite uniformly, although a clear overdensity is located in the inner region of the galaxy, specially inside one effective radius.

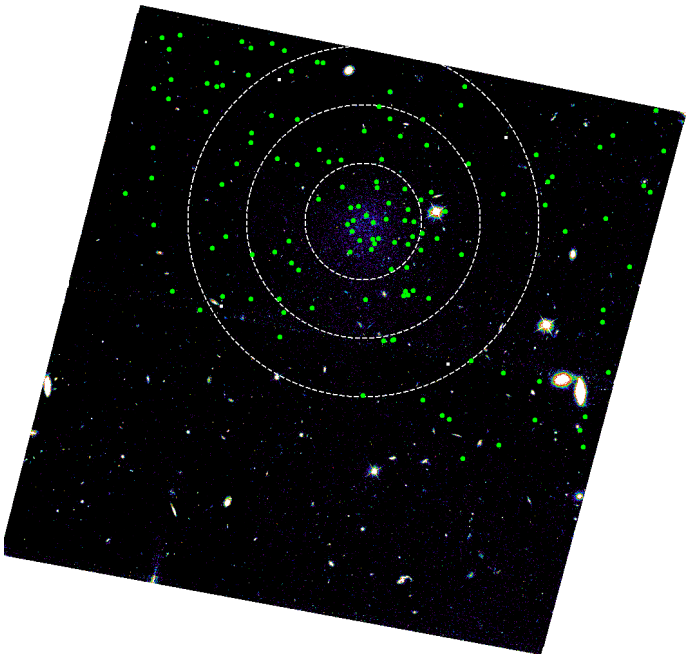

Figure 4.3: Sources locations (green dots) after selecting by effective radius, ellipticity and magnitude. white circles indicate one, two and three effective radius of the galaxy (17.″2, Müller et al. 2021). A distribution quite uniform with a overdensity in the inner parts of the galaxy is found. The distance assumed is 21 Mpc.

4.2 Colour selection

The GC candidates obtained in the previous section are now filtered by their colours. For this, the criteria defined in section 3.5.2 is applied. For a visual reference, Figure 4.4 and 4.5 shows the colour-colour diagram of all the sources which fulfill the effective radius, ellipticity and magnitude conditions.

The section that the confirmed GC occupy is narrow, specially using the aperture photometry. There are a lot of candidates with colours really different, meaning that even if they fulfill the effective radius, ellipticity and magnitude criteria, they are not likely globular clusters.

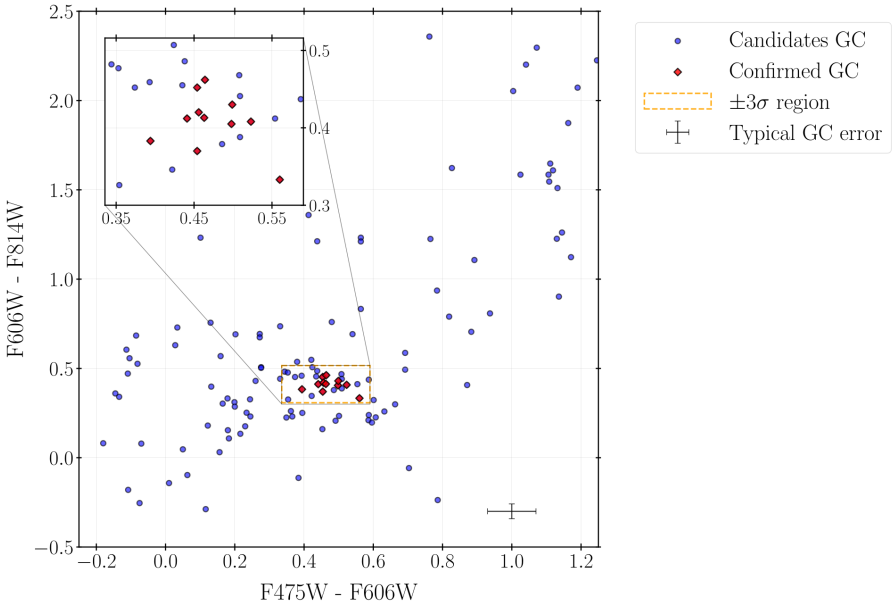

Figure 4.4: Colour-colour diagram using SExtractor's `MAG_AUTO`. In red the spectroscopically confirmed globular clusters are shown, in blue the preliminary sample. The error of a typical GC (a GC whose magnitude is that of the peak of the GCLF) at 21 Mpc (Appendix B.4 for 26 Mpc) is indicated in the black errorbars of the bottom right corner. The selection region is indicated in orange and is zoomed in the upper left corner for ease of viewing.

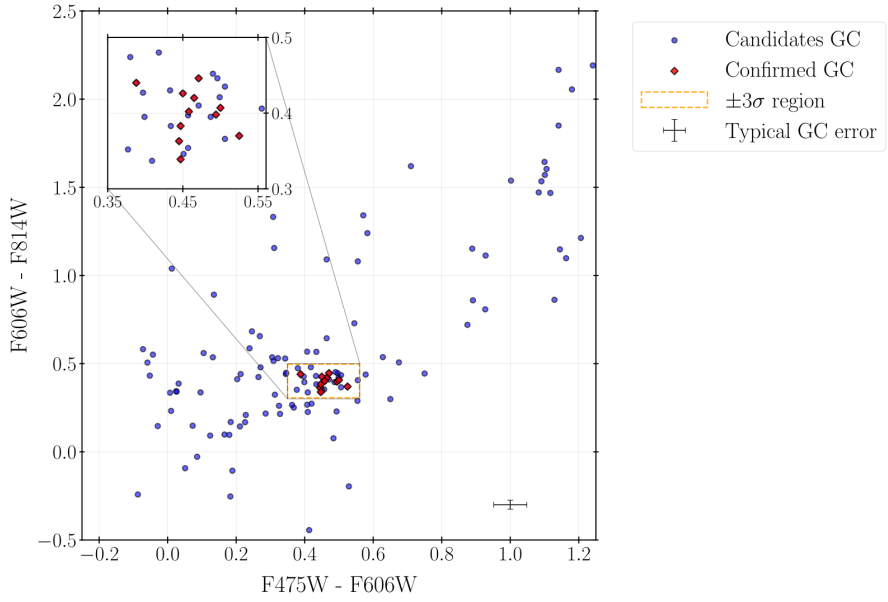

Figure 4.5: Colour-colour diagram using GC oriented aperture photometry. In red the confirmed spectroscopically globular clusters are shown, in blue the preliminary sample. The error of a typical GC (a GC whose magnitude is that of the peak of the GCLF) at 21 Mpc (Appendix B.4 for 26 Mpc) is indicated in the black errorbars of the bottom right corner. The selection region is indicated in orange and is zoomed in the upper left corner for ease of viewing.

The final selection of GCs consists on 26 sources using `MAG_AUTO` or 30 sources using aperture photometry, assuming 21 Mpc. At 26 Mpc, 26 and 29 sources are found, respectively. All photometric properties are compiled in Appendix C.

We visually inspect the spatial distribution of the GC candidates in Figure 4.6 (Appendix B.5 for 26 Mpc candidates). The green circles are candidates obtained independently of applying automatic or aperture photometry, in yellow and red are the candidates that are only detected with automatic and aperture photometry respectively.

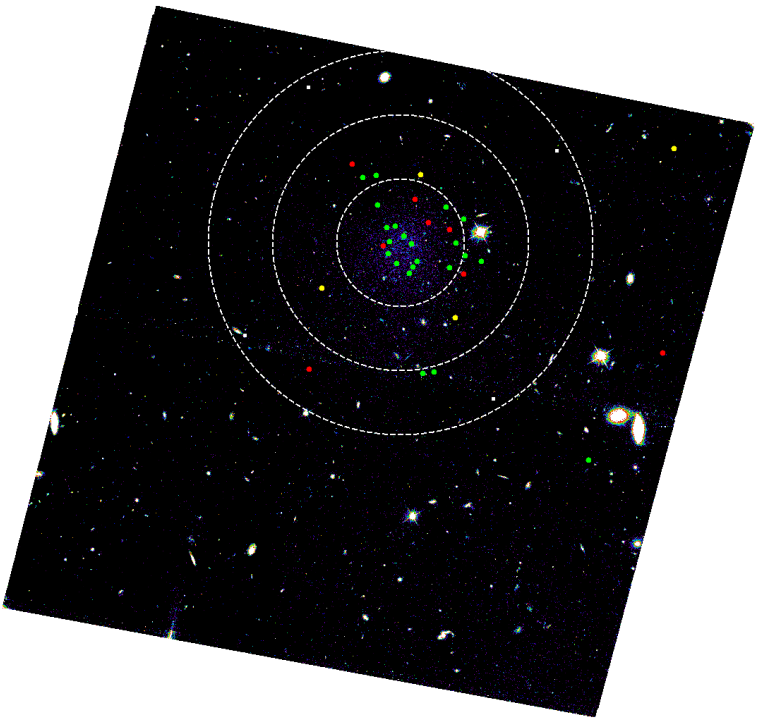

Figure 4.6: GC candidates after selecting by effective radius, ellipticity, magnitude and colour. White circles indicate one, two and three effective radius ($17\farcs2$, Müller et al. 2021) of the galaxy MATLAS-2019. The green circles are the candidates obtained independently of the photometry used, in yellow are candidates only detected with `MAG_AUTO` and in red candidates only detected with photometry mode. Results assuming a distance to the galaxy of 21 Mpc.

Most of the GC candidates are located inside two effective radius from the center of the galaxy. Also, there are some candidates outside three effective radius. In addition, there are two candidates in the gap between CCDs, which is a noisy region. The distant candidates and those of the gap are suspicious due to their location and may not be globular clusters of the galaxy.

One of the things that stand out when looking at the distribution of GC candidates is the overdensity on the west side of the galaxy (right side of the image, towards the bright star). Around 10 sources are located in this region.

4.3 Analysis of globular cluster population

After selecting by effective radius, ellipticity, magnitude and colours a population of globular cluster candidates has been obtained. Now, some checks to the GC candidates are performed to make sure that the population is reasonable, thus being able to know if our selection process has been adequate.

4.3.1 Globular Cluster Luminosity Function

The first thing to check is the globular cluster luminosity function (GCLF). As said before, the distribution of globular cluster magnitudes appears to be universal, so we have a hint of what distribution of magnitudes our selection should have.

The GCLF for the GC candidates with `MAG_AUTO` and aperture photometry are shown in Figure 4.7 for 21 Mpc (Appendix B.6 for 26 Mpc results). Both of them show reasonable well the typical GCLF behaviour, this is, a Gaussian shape. It has to be taken into account the relatively small number of sources (30 or less), so there can be statistical effects in the exact distribution of these magnitudes.

The confirmed GCs are the bright tail of the population, even though some other bright sources are detected out of the field studied spectroscopically. Also, from the comparison of the GCLF at 21 Mpc and 26 Mpc, a distance around 21 Mpc seems too be more representative of the real distance. This way, from now on, we will work assuming a distance of 21 Mpc.

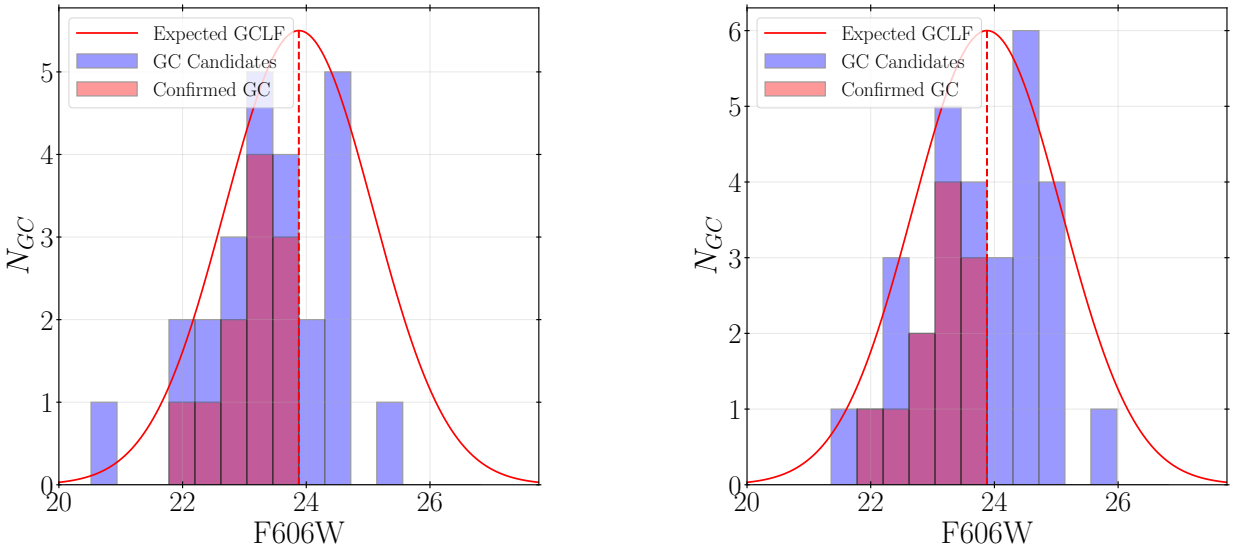

Figure 4.7: GCLF for the final GC candidates. The left plot is the GCLF obtained using automatic photometry and the right one is obtained using aperture photometry. The vertical dashed line represents the expected turnover magnitude for a distance of 21 Mpc.

4.3.2 Effective radius distribution

Next, the effective radius distribution of the GC candidates is checked. We have selected sources with effective radii from 0 up to 10 parsecs, based of the analysis of the Harris' and Georgiev's catalogues and the confirmed GCs of MATLAS-2019.

In Figure 4.8 the histogram of effective radii is shown. Most of the GC candidates are between 3 and 5 parsecs. This is what we would expect if the objects selected are real GCs, given that the mean radius obtained in section 3.1.2 was around 3.6 pc.

There are some big and small GC candidates. Using `MAG_AUTO` the sources are more scattered, this is, bigger and smaller sources. The aperture photometry produces a more clustered population around 3 to 5 parsecs. In general it seems a reasonable effective radius distribution for a GC population.

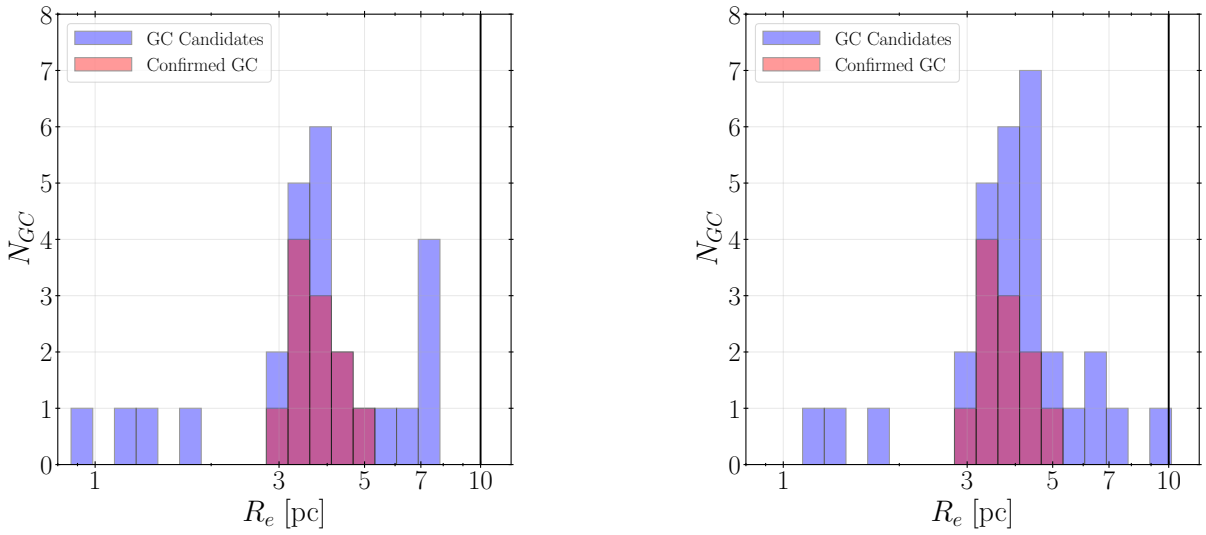

Figure 4.8: Effective radius distribution of the final GC candidates. The left plot are the effective radii of automatic photometry candidates and the right one of aperture photometry candidates. The vertical black line is the upper limit for the effective radius selection.

4.3.3 Radial profile

Another interesting analysis to perform to the GC candidates is its radial extension. This analysis will allow us to know how the density of globular clusters behaves and how far it extends from the center of the galaxy. For this, the distribution of the distance of the GCs to the center of the galaxy and the radial profile is going to be computed.

First, we measured the distances to the center of the galaxy for each candidate. This information is shown as a histogram in the left plot of Figure 4.9. We measure the number of GCs in a set of concentric rings up to 55 arcsecs. From these, the number of globular clusters per area has been calculated. The width of the rings has been fixed to 5 arcsec, which is around $\frac{1}{3}\, r_{eff}$. The resulting profile can be seen in the right plot of Figure 4.9.

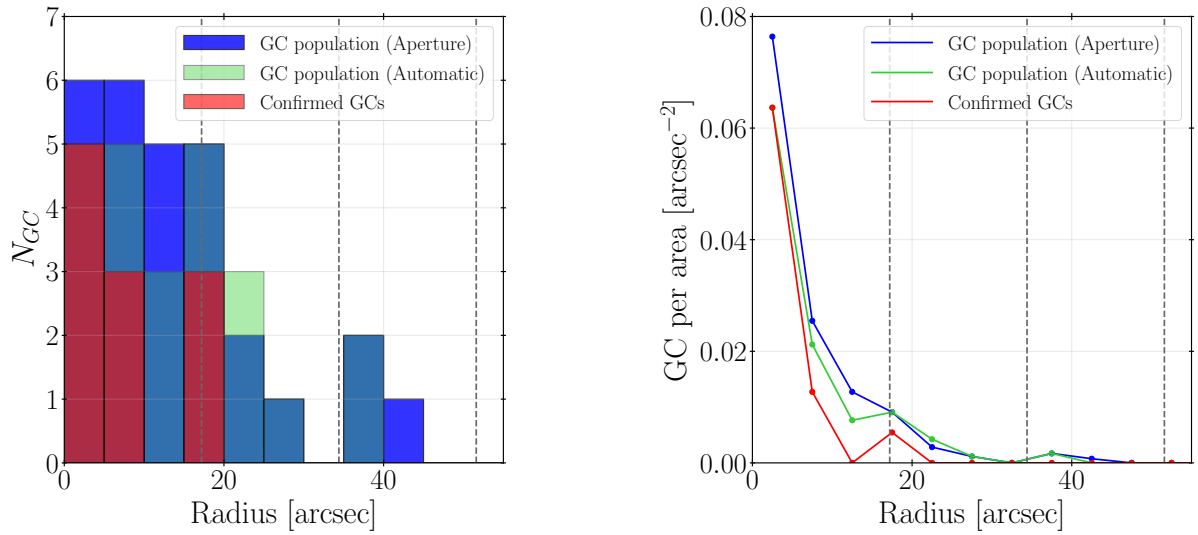

Figure 4.9: Radial distribution of globular clusters. In red the data for spectroscopically confirmed GC and in green and blue the GC populations obtained with automatic and aperture photometry (respectively). Grey vertical lines indicates one, two and three efective radius. Left: The radial distances of the GCs to the center of the galaxy. Right: number density of GCs per area as a function of the radius.

The radial profile of the GC population resembles the radial profile of the confirmed GC population. Also, the difference between the population obtained with automatic photometry and with aperture photometry is small. The general shape does not vary between them.

Regarding the radial distribution as a function of the effective radius, is found that at 1 effective radius, the density of globular clusters is around a 12% or 14% (depending on the photometry applied) that of the inner most circle. At two effective radius the density profile has reached 0, even though some isolated GC candidates are found outside of this radius (sources mentioned above, suspicious given their distance from the galaxy and their position in the gap).

The GC half-number radius (i.e., the radius containing half of the globular clusters, $R_{e,GC}$) is $13.5 \pm 0''.1$ for aperture photometry candidates and $14.9 \pm 0''.1$ for automatic photometry candidates. Comparing these values with the effective radius of the galaxy ($17''.2$) we find $R_{e,GC}/R_e \approx 0.78$ for aperture photometry-based results and $R_{e,GC}/R_e \approx 0.86$ for automatic photometry-based results. What these values indicate is that the GC system is less extended than the stellar light component of the galaxy. These ratios for MATLAS-2019 are in line with other UDGs and other dwarf galaxies (Amorisco et al. 2018).

4.3.4 Total mass of MATLAS-2019

Once the catalogue of GC candidates has been obtained, the total mass (halo mass) of the galaxy is calculated. This is one of the important things to infer from the number of globular clusters and will give us an insight about the origin of the galaxy.

Different authors have calibrated the globular cluster-halo mass relation. We will use here two of the most recent calibrations to compute the mass of the halo.

Harris et al. (2017) found that, the ratio between the mass of the globular cluster system and the total mass is given by $M_{GCs}/M_h = 2.9 \times 10^{-5}$. For obtaining the total mass of the GC system a mean GC mass of $1.0 \times 10^5 M_\odot$ is assumed (again, Harris et al. 2017).

This way, with the results obtained from automatic photometry (26 GC) the total mass for the GC system is $2.6 \times 10^6 M_\odot$. This implies a halo mass of $M_{halo} = 8.96 \times 10^{10} M_\odot$. The calculations for the aperture photometry (30 GC) are $3 \times 10^6 M_\odot$ for the M_{GCs} and $1.03 \times 10^{11} M_\odot$ for the halo mass.

Spitler and Forbes (2009) found a slightly different relation, expressed as $log(M_{halo}) = log(M_{GCs}) + 4.15$. They assume a mean GC mass of $4.0 \times 10^5 M_\odot$, so we will use this value as well. In this case, a halo mass of $1.47 \times 10^{11} M_\odot$ is found for automatic photometry and a halo mass of $1.69 \times 10^{11} M_\odot$ for aperture photometry.

In both cases, the estimations of the halo masses for the galaxy are similar, this is, around $10^{11} M_\odot$.

Chapter 5

Discussion and conclusions

In this last chapter the results found on the MATLAS-2019 globular cluster system are discussed and compared with the results obtained in other studies. Then, a conclusion and some final thoughts will be presented as well.

Regarding the globular cluster system, we might wonder whether this galaxy is truly an outlier in terms of the number of globular clusters or whether it has a typical GC population for an Ultra Diffuse Galaxy. The GC populations of some UDGs have been already studied. For example, Forbes et al. (2020) studied 85 UDGs in the Coma cluster. He found that Coma UDGs show an overabundance in GCs compared with early-type dwarfs and local dwarfs of a similar stellar mass, even though LSB dwarfs from Coma showed a similar overabundance. So it seems that this rich GC population in the context of dwarf galaxies is not something exclusive of Ultra Diffuse Galaxies. In the study, 72% of the UDGs have less than 30 GCs and 82% have less than 40 GCs.

This agrees with the results obtained, where 26 or 30 globular clusters are obtained depending on the photometry used. Moreover, our GC selection has some suspicious candidates really far from the center of the galaxy (outside 2 and 3 effective radius) and in the gap region. This implies that some of these sources are likely to be interlopers and our final population may be closer to 25 candidates.

The GC system that is found in this study agrees with the result found by Müller et al. (2020), this is, 26 ± 6 globular clusters. Muller et al. globular cluster selection is based in a first filtering by ellipticity, magnitude and color criteria. Then, a Markov Chain Monte Carlo (MCMC) algorithm is applied to estimate the real number of GCs. The amount of globular clusters that have been found in this work is within the errors of that study.

However, Danieli et al. (2022) found 54 ± 9 globular clusters. This would imply that MATLAS-2019 is one of the UDGs with the richest GC system. Danieli et al. GC selection is based in FWHM and color criteria obtained from the study of the spectroscopically confirmed GC of the galaxy. This is a methodology similar to that of our study, but the results do not match.

Clearly, the next question is: Where does this difference between the results of Danieli et al.'s study and ours come from? Well, the first fact to take into account is that they only have two filters (*F475W* and *F606W*), which means that they have only one colour. Considering that colour is the most restrictive criterion, filtering with two colours, as done in this study, narrows down even more the selection. It is true that Müller et al. (2020) also uses only one colour, but the methods applied in that study are considerable different from those applied here, making a direct comparison difficult.

The availability of two colours is not the only reason for the difference in the number of GCs found. The selection criteria is also quite different. The colour range used by Danieli et al. (2022) for filtering the globular cluster candidates is more generous than ours, with a criterion that varies depending on the magnitude: for bright sources a colour cut from $0.2 < F475W - F606W < 0.6$ magnitudes is applied, and for fainter sources from $0.08 < F475W - F606W < 0.8$ magnitudes. No justification is provided for these criteria and, comparing these ranges with the used in this work ($0.35 < F475W - F606W < 0.56$) shows one of the main reasons why the number of GC candidates differs.

Another point to consider is that in this work and in the one carried out by Müller et al. the ellipticity is taken into account and objects with ellipticities higher than 0.2 are rejected. Danieli et al. imposes no restrictions on ellipticity.

Finally, the distance assumed to the galaxy also makes a difference. Both in this analysis and in Müller et al., a distance of 21 Mpc is used, making the completeness correction negligible. However, Danieli et al. assumes the farthest possible distance for the galaxy, this is, 26.5 Mpc. This introduces a completeness correction that is not decisive but also contributes to increase the number of GC candidates.

It should be noted that the smaller number of candidates obtained in this study can not be attributed to the construction of the catalog since in all cases it has been built using SExtractor and a lower detection threshold (3 in Müller at al. study, 2 in Danieli's et al. study and 1.3 in this study) as well as a lower minimum number of pixels for detection (6 in Danieli's et. al study, 5 in Müller et al. study and 5 in this study) were employed.

Our analysis support that MATLAS-2019 hosts a reasonable GC system for an UDG. Nevertheless, as stated before, that does not mean that it is not a rich GC population compared with other dwarf galaxies.

Moreover, the distribution of GCs is unusual. In Figure 5.1 the inner part of the galaxy is shown. Red cricles are spectroscopically confirmed GC and yellow circles are GC candidates obtained in this study. Even though the light distribution of the galaxy seems reasonable symmetrical, the distribution of globular clusters is not. There is a larger amount of globular clusters on the west (right side of the image).

Looking to the region of the sky in which MATLAS-2019 is located using deep data from the *Legacy Surveys* [1], no objects are found that could cause the observed asymmetry. Moreover, the bright star that does not allow us to see if something is happening in that side of the galaxy. Is this distribution a coincidence or maybe the galaxy is undergoing some sort of interaction that we are not able to see because of the star? If this is really produced by some interaction, it would also be necessary to explain why only the distribution of the GCs is affected and not the diffuse light of the galaxy.

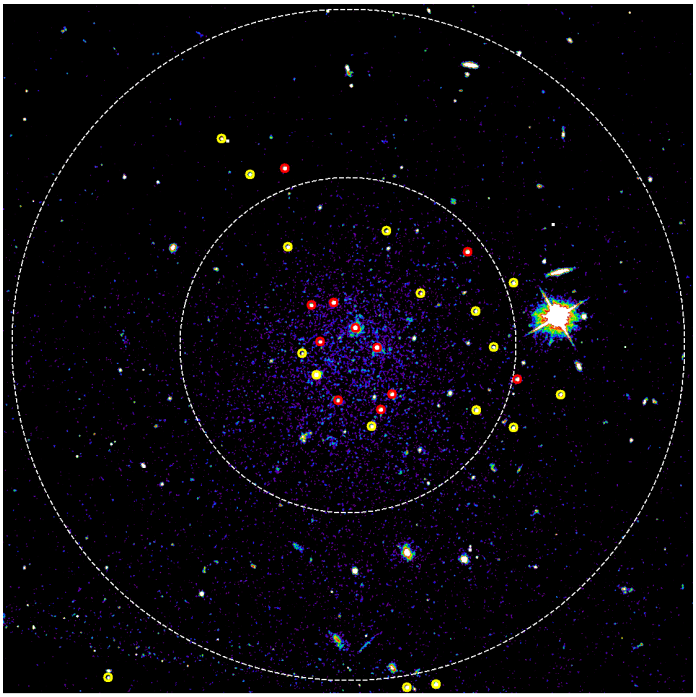

Figure 5.1: Inner region of MATLAS-2019. The spectroscopically confirmed GC and the GC candidates obtained with aperture photometry are indicated (red and yellow circles respectively). In white is indicated one and two effective radius. The GC distribution is not symmetrical.

[1] https://www.legacysurvey.org/

Spectroscopy would be the only way to confirm the candidates and find out if the excess is real or product of background contamination. Nonetheless some already spectroscopically confirmed GCs seem to be located in that region.

In Figure 5.2 a plot taken from Forbes et al. (2018) is shown. The plot shows the globular cluster-halo mass relation that they find. In blue and red there are different dwarfs galaxies (rotationally supported and pressure supported respectively) and the black dots are galaxies of all kind of masses. The black line represent the fit to the data that they find and in grey the region where MATLAS-2019 is located based on the GC system found in this study.

Assuming that the total mass of MATLAS-2019 is located on top of the relationship of Forbes et al. (2018), it would imply a mass of $\sim 10^{11} M_{\odot}$. That would be on the higher mass end for a dwarf galaxy, but not anomalous. This can give us an idea about the nature of MATLAS-2019. Considering the issue surrounding the origin of UDGs, as discussed in the Introduction, it leads us to question whether this particular dwarf galaxy has undergone some process resulting in a UDG galaxy or it represents a failed galaxy embedded within a massive dark matter halo. MATLAS-2019 for sure have a rich GC population but (assuming the current GC-HM relations) it does not seem to correspond to an unexpectedly massive halo, being consistent with belonging to dwarf galaxies.

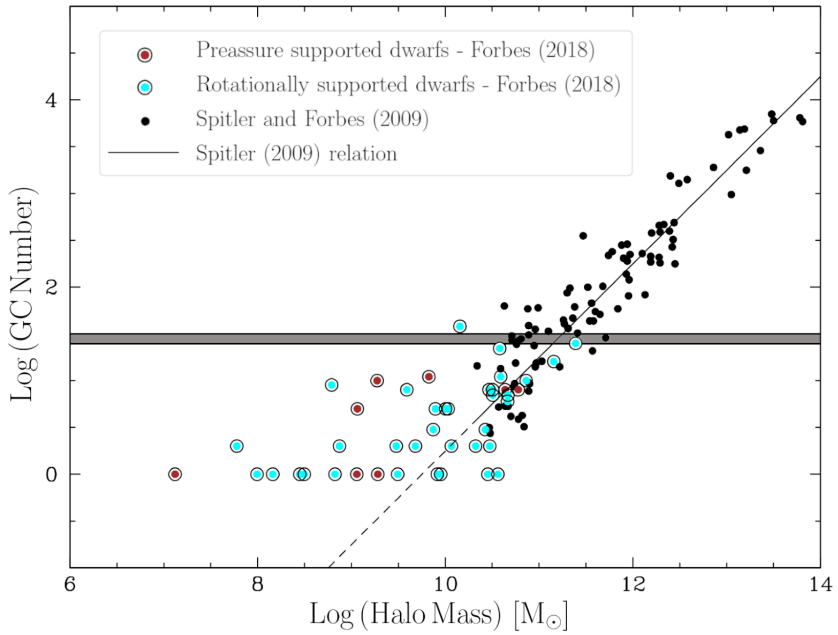

Figure 5.2: Globular cluster-Halo mass relation plot from Forbes et al. (2018). In blue and red are shown dwarf galaxies rotationally and pressure supported respectively. Black dots represent a wide variety of galaxies and the solid line represents the GC-HM relation. The grey region is the location in which MATLAS-2019 is located assuming the number of GC found in this study.

Our results shed additional light on the issue of the globular cluster population of MATLAS-2019, complementing and confirming previous studies on the subject by using more information and parameters for GC selection. We have done our best to ensure that all parts and decisions of the study are well argued and justified, reducing possible errors or biases. Thus, given the contentious situation of some studies with different results, this work appears to tip the scale towards a population of approximately 25 globular clusters.

The number of globular clusters provides information regarding the origin of Ultra Diffuse Galaxies. The results found here seems to favor the scenario in which these are not failed massive galaxies which reside in massive dark matter halos, but rather the low surface brightness and large effective radius tail of the abundant population of dwarf galaxies, whose properties were produced by a lack of recent star formation or by undergoing different processes that has puffed them up.

More work is currently being done to improve the quality of the study and confirm more robustly the findings presented here. We are developing simulations for studying the completeness as well as the inclusion of a new GTC image in the u-band to better clean the final GC sample.

However, we must be aware that this photometry-based method of detecting globular clusters is not perfect. Undoubtedly, we invested our best efforts to reliably detect the globular cluster population, but the true answer will come when a deep spectroscopic study is performed to MATLAS-2019.

New and intriguing questions regarding the distribution of globular clusters in MATLAS-2019 have arisen. Is the galaxy undergoing some kind of interaction? How can we explain the asymmetric distribution of globular clusters? Why is the diffuse body of the galaxy not being affected in the same way? A specific study addressing these questions must be conducted to provide answers.

In either case, what we can be certain of is that our knowledge still has some gaps when it comes to Ultra-Diffuse Galaxies, and many endeavors need to be undertaken to get closer to how the universe is.

Bibliography

M. Akhlaghi and T. Ichikawa. Noise-based Detection and Segmentation of Nebulous Objects. , 220(1):1, Sept. 2015. doi: 10.1088/0067-0049/220/1/1.

N. C. Amorisco, A. Monachesi, A. Agnello, and S. D. M. White. The globular cluster systems of 54 coma ultra-diffuse galaxies: statistical constraints from HST data. *Monthly Notices of the Royal Astronomical Society*, 475(3): 4235–4251, jan 2018. doi: 10.1093/mnras/sty116. URL https://doi.org/10.1093%2Fmnras%2Fsty116.

J. Binney and S. Tremaine. *Galactic Dynamics: Second Edition*. 2008.

N. Choksi and O. Y. Gnedin. Origins of scaling relations of globular cluster systems. , 488(4):5409–5419, Oct. 2019. doi: 10.1093/mnras/stz2097.

S. Danieli, P. van Dokkum, S. Trujillo-Gomez, J. M. D. Kruijssen, A. J. Romanowsky, S. Carlsten, Z. Shen, J. Li, R. Abraham, J. Brodie, C. Conroy, J. S. Gannon, and J. Greco. NGC 5846-UDG1: A Galaxy Formed Mostly by Star Formation in Massive, Extremely Dense Clumps of Gas. , 927(2):L28, Mar. 2022. doi: 10.3847/2041-8213/ac590a.

K. El-Badry, E. Quataert, D. R. Weisz, N. Choksi, and M. Boylan-Kolchin. The formation and hierarchical assembly of globular cluster populations. *Monthly Notices of the Royal Astronomical Society*, 482(4):4528–4552, 11 2018. ISSN 0035-8711. doi: 10.1093/mnras/sty3007. URL https://doi.org/10.1093/mnras/sty3007.

D. A. Forbes, J. I. Read, M. Gieles, and M. L. M. Collins. Extending the globular cluster system-halo mass relation to the lowest galaxy masses. , 481(4):5592–5605, Dec. 2018. doi: 10.1093/mnras/sty2584.

D. A. Forbes, J. Gannon, W. J. Couch, E. Iodice, M. Spavone, M. Cantiello, N. Napolitano, and P. Schipani. An ultra diffuse galaxy in the NGC 5846 group from the VEGAS survey. , 626:A66, June 2019. doi: 10.1051/0004-6361/201935499.

D. A. Forbes, A. Alabi, A. J. Romanowsky, J. P. Brodie, and N. Arimoto. Globular clusters in Coma cluster ultra-diffuse galaxies (UDGs): evidence for two types of UDG? , 492(4):4874–4883, Mar. 2020. doi: 10.1093/mnras/staa180.

D. A. Forbes, J. S. Gannon, A. J. Romanowsky, A. Alabi, J. P. Brodie, W. J. Couch, and A. Ferré-Mateu. Stellar velocity dispersion and dynamical mass of the ultra diffuse galaxy NGC 5846_UDG1 from the keck cosmic web imager. *Monthly Notices of the Royal Astronomical Society*, 500(1):1279–1284, 10 2020. ISSN 0035-8711. doi: 10.1093/mnras/staa3289. URL https://doi.org/10.1093/mnras/staa3289.

I. Y. Georgiev, M. Hilker, T. H. Puzia, P. Goudfrooij, and H. Baumgardt. Globular cluster systems in nearby dwarf galaxies - II. Nuclear star clusters and their relation to massive Galactic globular clusters. , 396(2):1075–1085, June 2009. doi: 10.1111/j.1365-2966.2009.14776.x.

R. Habas, F. Marleau, P.-A. Duc, P. Durrell, S. Paudel, M. Poulain, R. Sanchez-Janssen, S. Sreejith, J. Ramasawmy, B. Stemock, C. Leach, J.-C. Cuillandre, S. Gwyn, A. Agnello, M. Bilek, J. Fensch, O. Muller, E. Peng, and R. van der Burg. Newly discovered dwarf galaxies in the matlas low-density fields. *Royal Astronomical Society. Monthly Notices*, 491(2):1901–1919, Jan. 2020. ISSN 0035-8711. doi: 10.1093/mnras/stz3045.

W. E. Harris. A New Catalog of Globular Clusters in the Milky Way. *arXiv e-prints*, art. arXiv:1012.3224, Dec. 2010. doi: 10.48550/arXiv.1012.3224.

W. E. Harris, J. P. Blakeslee, and G. L. H. Harris. Galactic Dark Matter Halos and Globular Cluster Populations. III. Extension to Extreme Environments. , 836(1):67, Feb. 2017. doi: 10.3847/1538-4357/836/1/67.

B. W. Holwerda. Source extractor for dummies v5, 2005.

A. Mahdavi, N. Trentham, and R. B. Tully. The ngc 5846 group: Dynamics and the luminosity function to mr = 12. *The Astronomical Journal*, 130(4):1502, oct 2005. doi: 10.1086/444560. URL https://dx.doi.org/10.1086/444560.

S. S. McGaugh and J. Wolf. Local group dwarf spheroidals: Correlated deviations from the baryonic tully–fisher relation. *The Astrophysical Journal*, 722(1):248, sep 2010. doi: 10.1088/0004-637X/722/1/248. URL https://dx.doi.org/10.1088/0004-637X/722/1/248.

H. Mo, F. C. van den Bosch, and S. White. *Galaxy Formation and Evolution*. 2010.

O. Müller, F. R. Marleau, P.-A. Duc, R. Habas, J. Fensch, E. Emsellem, M. Poulain, S. Lim, A. Agnello, P. Durrell, S. Paudel, R. Sánchez-Janssen, and R. F. J. van der Burg. Spectroscopic study of MATLAS-2019 with MUSE: An ultra-diffuse galaxy with an excess of old globular clusters. , 640:A106, Aug. 2020. doi: 10.1051/0004-6361/202038351.

O. Müller, P. R. Durrell, F. R. Marleau, P.-A. Duc, S. Lim, L. Posti, A. Agnello, R. Sánchez-Janssen, M. Poulain, R. Habas, E. Emsellem, S. Paudel, R. F. J. van der Burg, and J. Fensch. Dwarf Galaxies in the MATLAS Survey: Hubble Space Telescope Observations of the Globular Cluster System in the Ultra-diffuse Galaxy MATLAS-2019. , 923(1):9, Dec. 2021. doi: 10.3847/1538-4357/ac2831.

E. W. Peng and S. Lim. A RICH GLOBULAR CLUSTER SYSTEM IN DRAGONFLY 17: ARE ULTRA-DIFFUSE GALAXIES PURE STELLAR HALOS? *The Astrophysical Journal*, 822(2):L31, may 2016. doi: 10.3847/2041-8205/822/2/l31. URL https://doi.org/10.3847%2F2041-8205%2F822%2F2%2Fl31.

M. Rejkuba. Globular cluster luminosity function as distance indicator. , 341(1):195–206, Sept. 2012. doi: 10.1007/s10509-012-0986-9.

T. Richtler. The globular cluster luminosity function: New progress in understanding an old distance indicator. In *Stellar Candles for the Extragalactic Distance Scale*, pages 281–305. Springer Berlin Heidelberg, 2003. doi: 10.1007/978-3-540-39882-0_15. URL https://doi.org/10.1007%2F978-3-540-39882-0_15.

T. Saifollahi, D. Zaritsky, I. Trujillo, R. F. Peletier, J. H. Knapen, N. Amorisco, M. A. Beasley, and R. Donnerstein. Implications for galaxy formation models from observations of globular clusters around ultra-diffuse galaxies. , 511(3):4633–4659, Apr. 2022. doi: 10.1093/mnras/stac328.

L. R. Spitler and D. A. Forbes. A new method for estimating dark matter halo masses using globular cluster systems. *Monthly Notices of the Royal Astronomical Society: Letters*, 392(1):L1–L5, 01 2009. ISSN 1745-3925. doi: 10.1111/j.1745-3933.2008.00567.x. URL https://doi.org/10.1111/j.1745-3933.2008.00567.x.

L. E. Strigari, S. M. Koushiappas, J. S. Bullock, M. Kaplinghat, J. D. Simon, M. Geha, and B. Willman. The most dark-matter–dominated galaxies: Predicted gamma-ray signals from the faintest milky way dwarfs. *The Astrophysical Journal*, 678(2):614–620, may 2008. doi: 10.1086/529488. URL https://doi.org/10.1086%2F529488.

M. A. Taylor, T. H. Puzia, R. P. Muñ oz, S. Mieske, A. Lançon, H. Zhang, P. Eigenthaler, and M. S. Bovill. The survey of centaurus a's baryonic structures (SCABS) – II. the extended globular cluster system of NGC 5128 and its nearby environment. *Monthly Notices of the Royal Astronomical Society*, 469(3):3444–3467, apr 2017. doi: 10.1093/mnras/stx1021. URL https://doi.org/10.1093%2Fmnras%2Fstx1021.

I. Trujillo. Ultra-diffuse galaxies at the crossroads. *Nature Astronomy*, 5(1184), Dec 2021. doi: 10.1038/s41550-021-01388-y.

P. G. van Dokkum, R. Abraham, A. Merritt, J. Zhang, M. Geha, and C. Conroy. Forty-seven Milky Way-sized, Extremely Diffuse Galaxies in the Coma Cluster. , 798(2):L45, Jan. 2015. doi: 10.1088/2041-8205/798/2/L45.

Appendix A

Photometry comparison

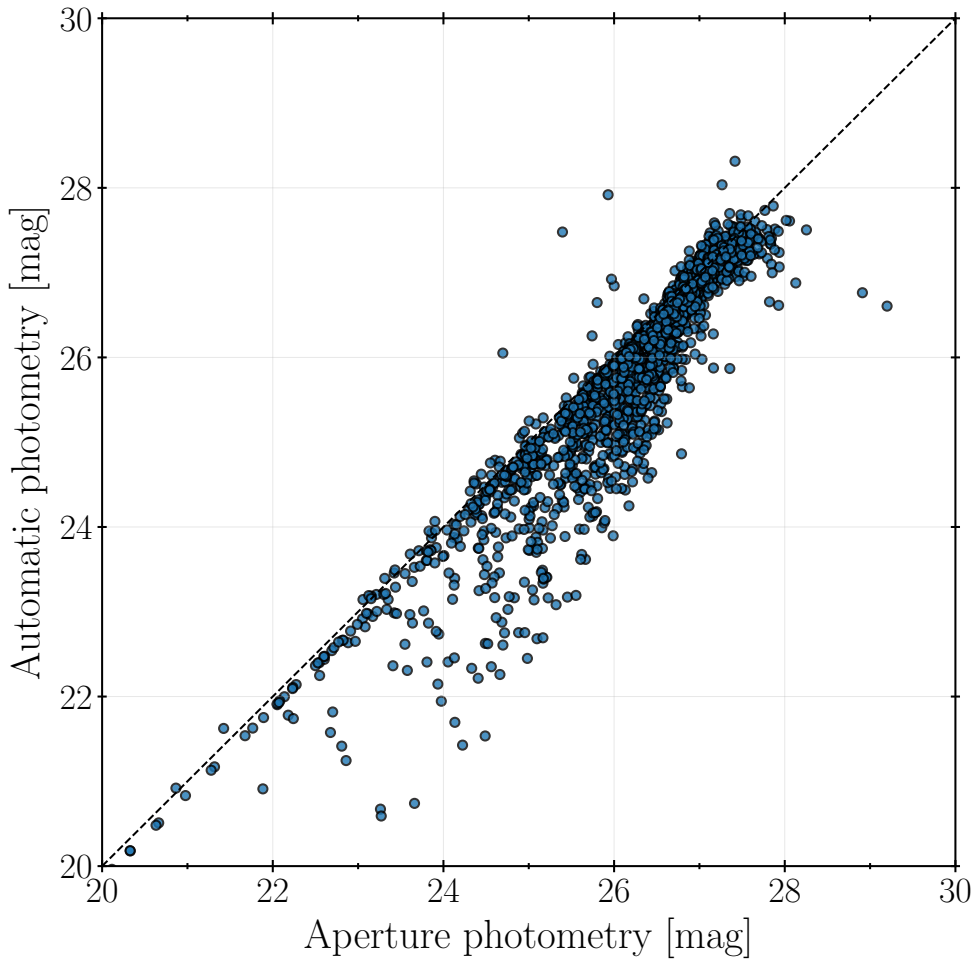

Figure A.1: Comparison between aperture photometry and automatic photometry, both of them corrected from Encircled Energy and Galactic extinction. The dashed black lines indicates what a perfect match would look like. There are some big differences (one or two magnitudes in some cases) due to big and extended objects that are not well measured with the aperture aperture.

Appendix B

Analysis assuming 26 Mpc

B.1 Confirmed spectroscopically globular cluster analysis

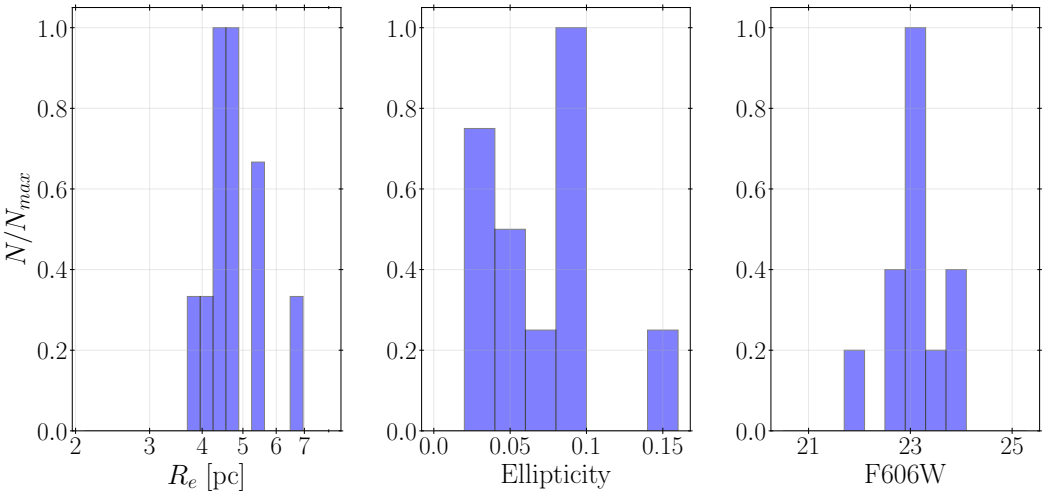

Figure B.1: Effective radius, ellipticity and magnitude distributions of the confirmed spectroscopically globular clusters using automatic photometry. The distance assumed for the effective radius is 26 Mpc.

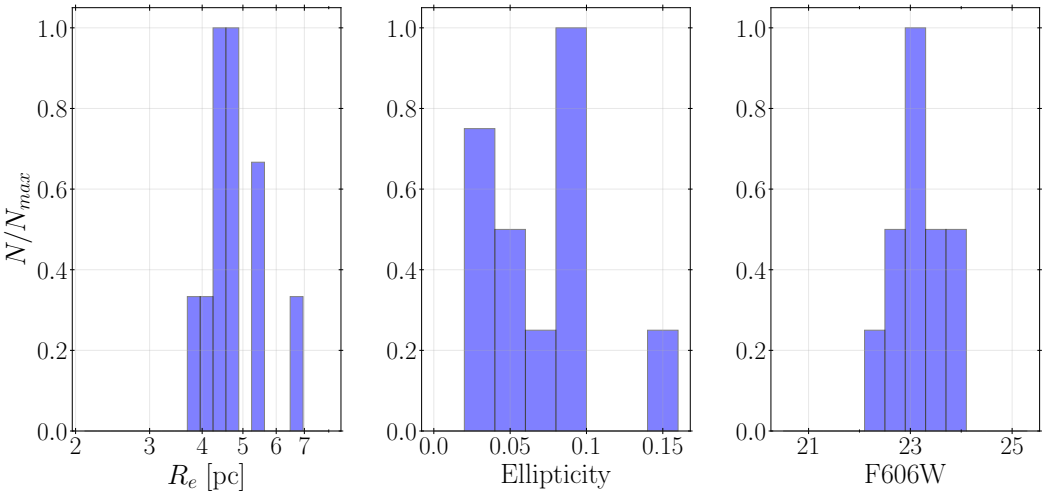

Figure B.2: Effective radius, ellipticity and magnitude distributions of the confirmed spectroscopically globular clusters using aperture photometry. The distance assumed for the effective radius is 26 Mpc.

B.2 Effective radius, ellipticity and magnitude filter histograms

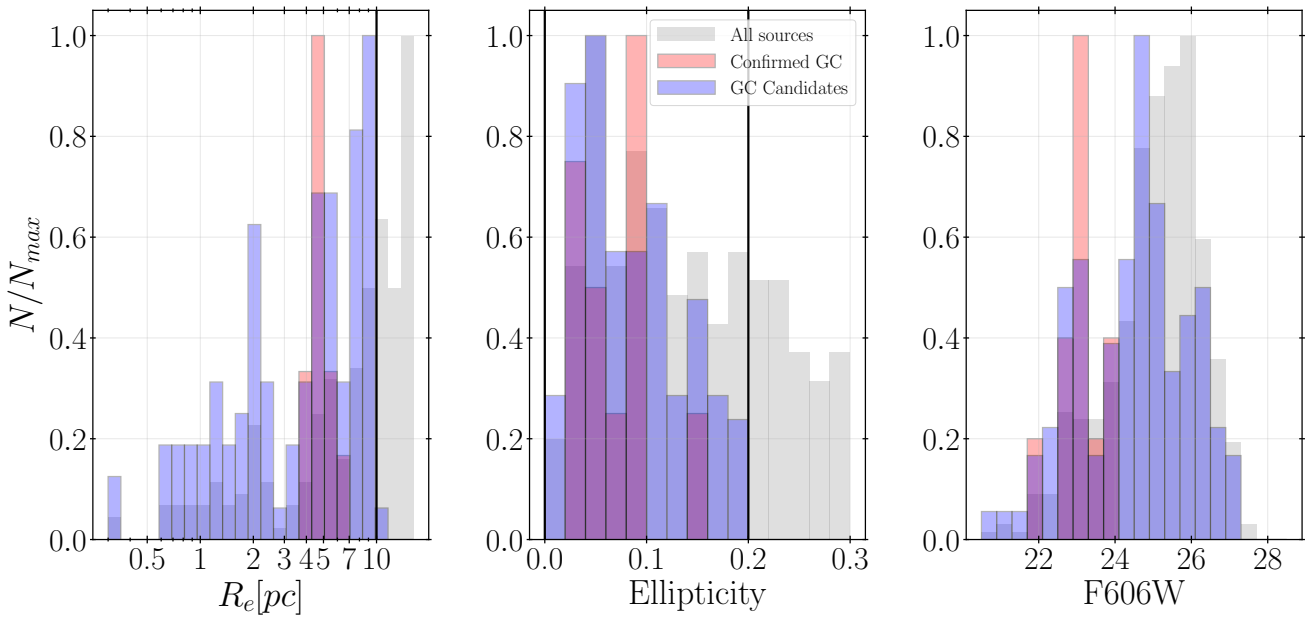

Figure B.3: Effective radius, ellipticity and magnitude (automatic photometry) distributions of differente samples of sources. In red the GCs confirmed spectroscopically , in blue the GC candidates (sources which fulfill all the conditions) and in gray all the sources of the catalogue. The vertical black lines are the ranges imposed in the GC selection. The assumed distance is 26 Mpc.

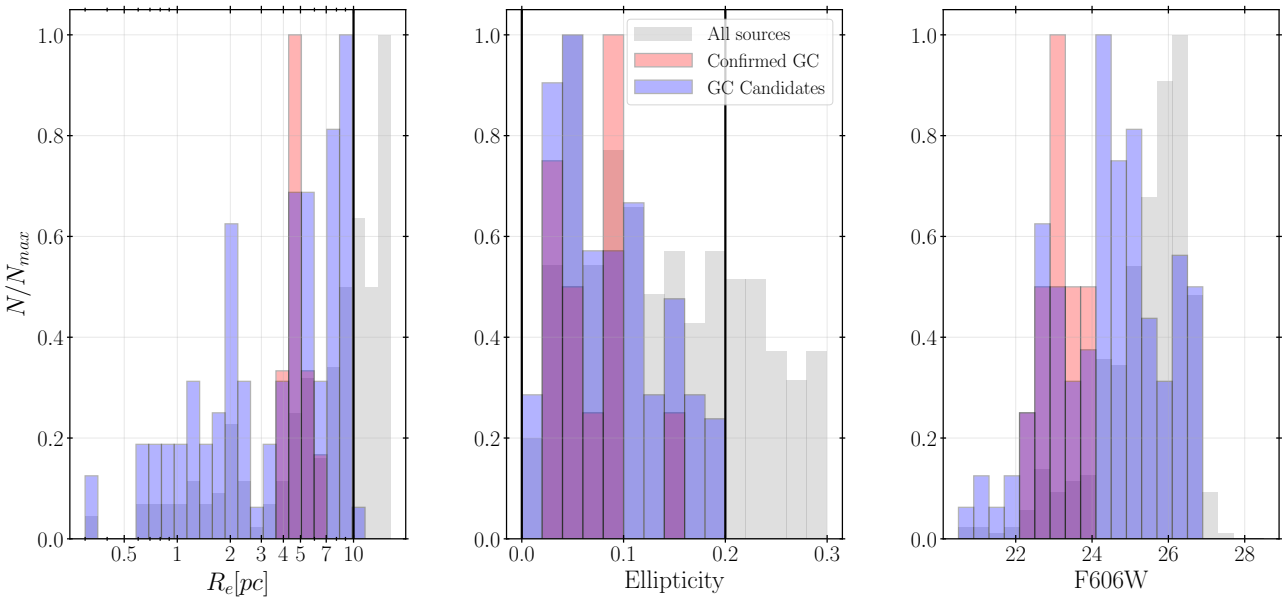

Figure B.4: Effective radius, ellipticity and magnitude (aperture photometry) distributions of differente samples of sources. In red the GCs confirmed spectroscopically , in blue the GC candidates (sources which fulfill all the conditions) and in gray all the sources of the catalogue. The vertical black lines are the ranges imposed in the GC selection. The assumed distance is 26 Mpc.

B.3 Effective radius, ellipticity and magnitude filter candidates

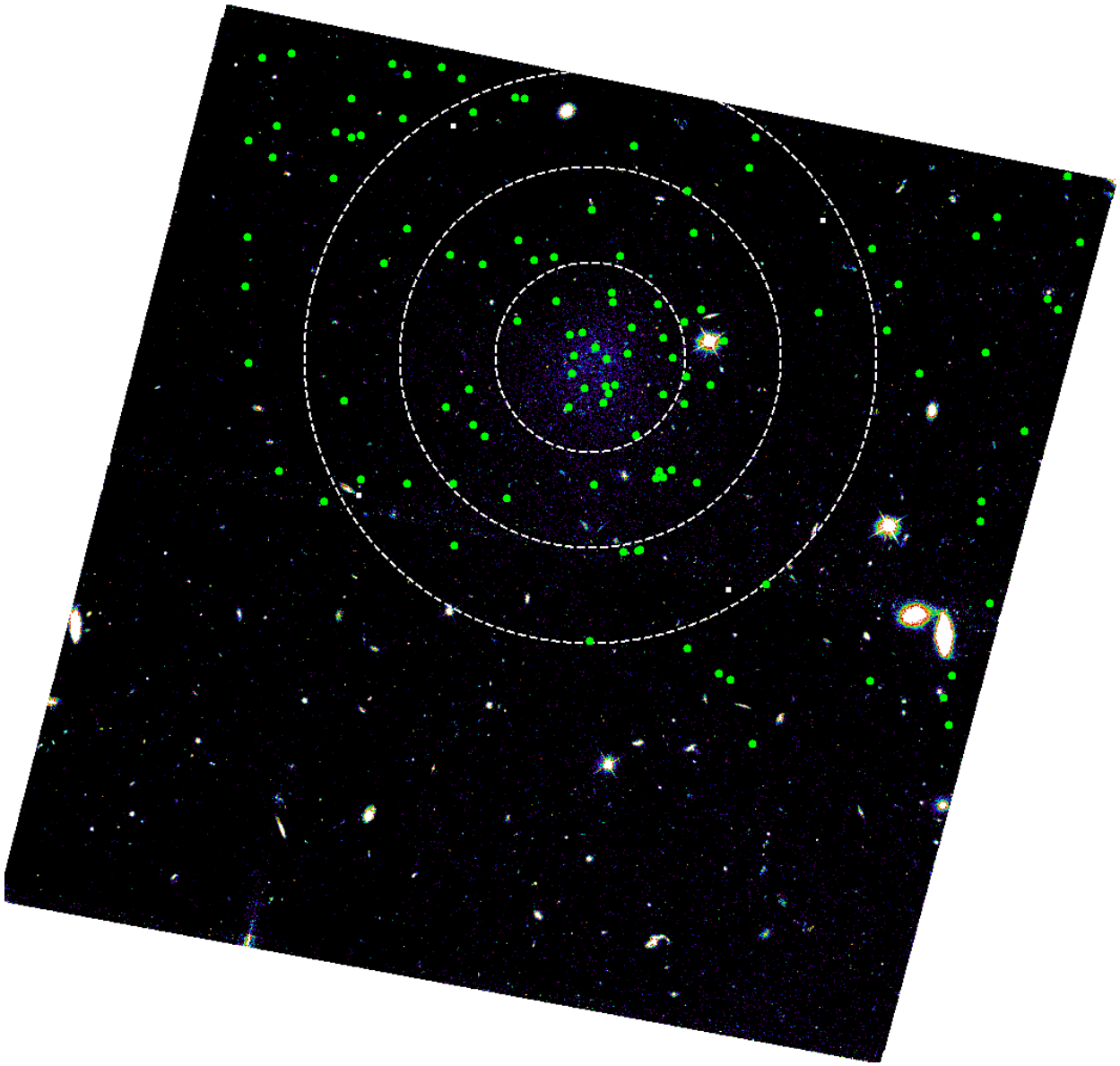

Figure B.5: GC candidates after filtering by effective radius, ellipticity and magnitude as green dots. White circles indicate one, two and three effective radius of the galaxy. A distribution quite uniform with a overdensity in the inner parts of the galaxy is found. These candidates are found independently of the photometry mode used The distance assumed is 26 Mpc.

B.4 Colour-colour diagram

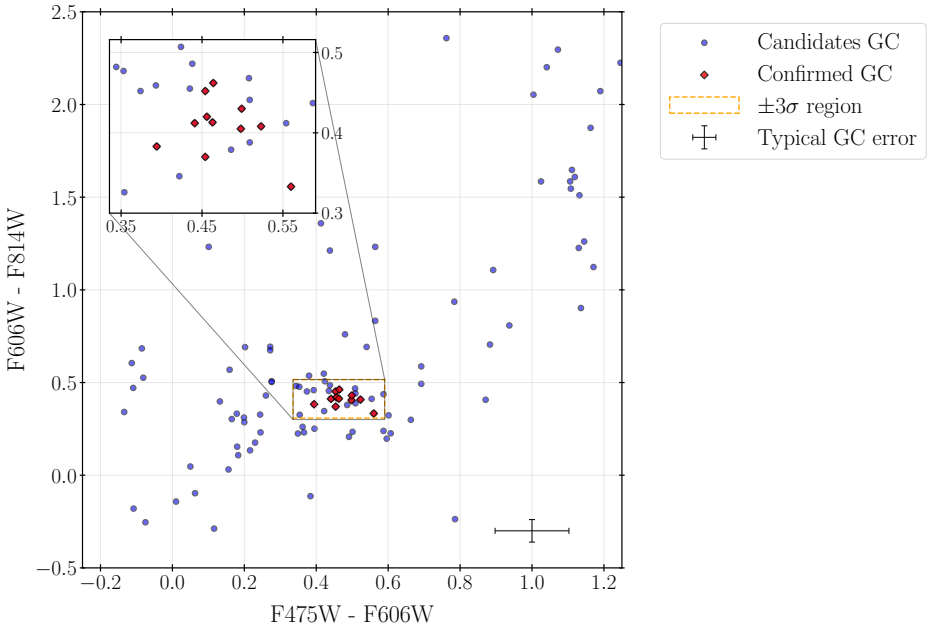

Figure B.6: Colour-colour diagram using SExtractor's `MAG_AUTO`. In red the spectroscopically confirmed globular clusters are shown, in blue the preliminary sample. The error of a typical GC (a GC whose magnitude is that of the peak of the GCLF) at 26 Mpc is indicated in the black errorbars of the bottom right corner. The selection region is indicated in orange and is zoomed in the upper left corner for ease of viewing.

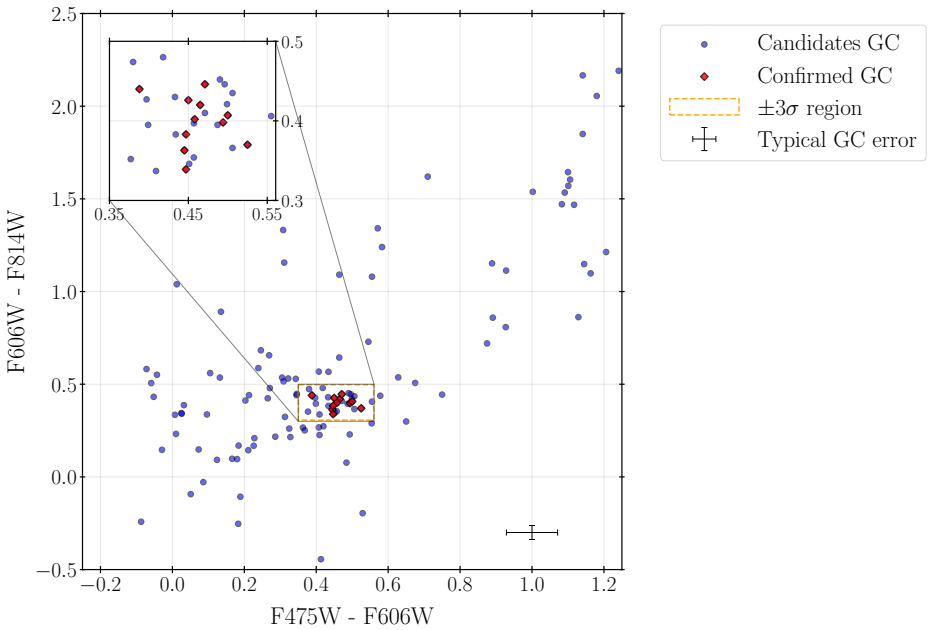

Figure B.7: Colour-colour diagram using GC oriented aperture photometry. In red the confirmed spectroscopically globular clusters are shown, in blue the preliminary sample. The error of a typical GC (a GC whose magnitude is that of the peak of the GCLF) at 26 Mpc is indicated in the black errorbars of the bottom right corner. The selection region is indicated in orange and is zoomed in the upper left corner for ease of viewing.

B.5 Colour filter candidates

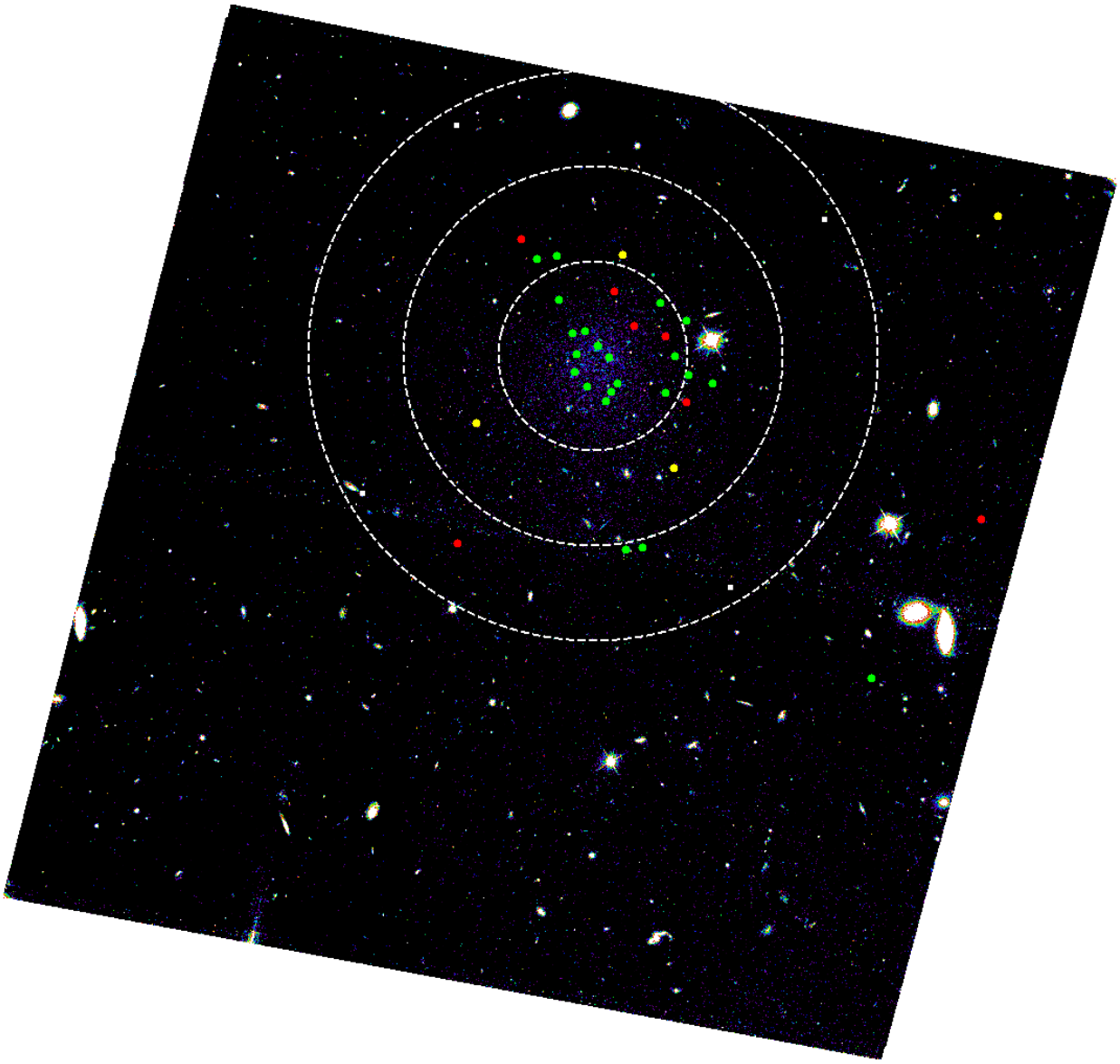

Figure B.8: GC candidates after filtering by effective radius, ellipticity, magnitude and colour. White circles indicate one, two and three effective radius of the galaxy. The green circles are candidates obtained independently of the photometry mode, in yellow are candidates only detected with automatic photometry and in red candidates only detected with photometry mode. Results for 26 Mpc.

B.6 Globular cluster luminosity function

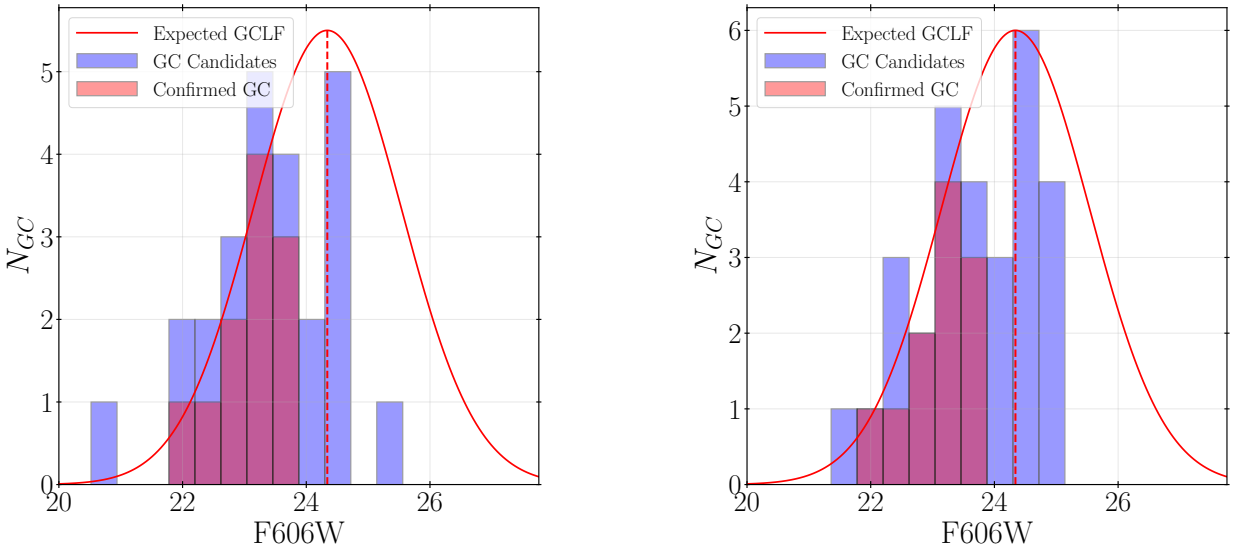

Figure B.9: GCLF for the final GC candidates. The left plot is the GCLF obtained using automatic photometry and the right one is obtained using aperture photometry. The vertical dotted line represents the expected turnover magnitude for a distance of 26 Mpc.

Appendix C

Parameters of GC candidates

Table C.1: GC candidates identified in MATLAS-2019. The magnitudes are obtained using SExtractor's automatic photometry and are corrected from Galactic Extinction. Asterisks indicate the spectroscopically confirmed globular clusters.

Name	RA (J2000.0)	Dec (J2000.0)	F475W (mag)	F606W (mag)	F814W (mag)	R_e (arcsec)	Ellipticity
GC0*	226.336544	1.817503	23.356 ± 0.020	22.893 ± 0.010	22.480 ± 0.011	0.034 ± 0.000	0.096 ± 0.017
GC1*	226.331357	1.815125	23.785 ± 0.030	23.262 ± 0.013	22.854 ± 0.015	0.038 ± 0.001	0.030 ± 0.018
GC2*	226.335160	1.813678	23.579 ± 0.025	23.081 ± 0.011	22.676 ± 0.012	0.037 ± 0.001	0.029 ± 0.018
GC3*	226.334535	1.812961	22.480 ± 0.010	22.039 ± 0.005	21.627 ± 0.005	0.052 ± 0.000	0.089 ± 0.013
GC4*	226.335797	1.813603	24.251 ± 0.046	23.795 ± 0.019	23.375 ± 0.020	0.033 ± 0.001	0.098 ± 0.020
GC5*	226.333920	1.812404	22.970 ± 0.015	22.506 ± 0.007	22.044 ± 0.008	0.042 ± 0.000	0.060 ± 0.016
GC6*	226.329937	1.811504	24.168 ± 0.042	23.608 ± 0.017	23.275 ± 0.018	0.038 ± 0.001	0.149 ± 0.019
GC7*	226.335548	1.812565	24.258 ± 0.046	23.864 ± 0.020	23.481 ± 0.021	0.030 ± 0.001	0.027 ± 0.020
GC8*	226.335655	1.811625	23.408 ± 0.021	22.909 ± 0.010	22.479 ± 0.011	0.043 ± 0.000	0.086 ± 0.017
GC9*	226.333500	1.811074	23.657 ± 0.027	23.203 ± 0.012	22.833 ± 0.014	0.034 ± 0.001	0.045 ± 0.018
GC10*	226.333823	1.810629	23.717 ± 0.028	23.263 ± 0.013	22.811 ± 0.014	0.034 ± 0.001	0.055 ± 0.018
GC11	226.314368	1.819458	21.355 ± 0.005	20.768 ± 0.000	20.331 ± 0.000	0.009 ± 0.000	0.047 ± 0.000
GC12	226.340596	1.809073	25.062 ± 0.092	24.627 ± 0.038	24.172 ± 0.038	0.077 ± 0.001	0.103 ± 0.026
GC13	226.333241	1.817537	25.774 ± 0.173	25.381 ± 0.075	24.922 ± 0.073	0.074 ± 0.003	0.101 ± 0.036
GC14	226.330691	1.806836	27.278 ± 0.368	26.925 ± 0.276	26.448 ± 0.271	0.068 ± 0.015	0.147 ± 0.080
GC15	226.337543	1.817332	24.900 ± 0.078	24.391 ± 0.032	24.003 ± 0.033	0.052 ± 0.001	0.080 ± 0.024
GC16	226.330051	1.814242	24.618 ± 0.062	24.132 ± 0.025	23.753 ± 0.025	0.033 ± 0.001	0.021 ± 0.021
GC17	226.336456	1.815258	23.912 ± 0.033	23.404 ± 0.014	22.936 ± 0.015	0.030 ± 0.001	0.007 ± 0.018
GC18	226.330619	1.812414	25.059 ± 0.091	24.621 ± 0.038	24.135 ± 0.037	0.037 ± 0.002	0.045 ± 0.026
GC19	226.328714	1.811063	24.684 ± 0.066	24.310 ± 0.029	23.858 ± 0.027	0.075 ± 0.001	0.106 ± 0.023
GC20	226.331104	1.810617	24.365 ± 0.050	24.021 ± 0.023	23.539 ± 0.021	0.065 ± 0.001	0.140 ± 0.021
GC21	226.335041	1.810901	24.950 ± 0.082	24.526 ± 0.036	24.019 ± 0.034	0.039 ± 0.002	0.067 ± 0.026
GC22	226.334080	1.810156	24.217 ± 0.044	23.863 ± 0.020	23.537 ± 0.021	0.040 ± 0.001	0.036 ± 0.020
GC23	226.320729	1.796235	22.440 ± 0.009	21.886 ± 0.005	21.474 ± 0.005	0.013 ± 0.000	0.025 ± 0.013
GC24	226.333080	1.802732	23.238 ± 0.018	22.729 ± 0.008	22.288 ± 0.008	0.018 ± 0.001	0.027 ± 0.016
GC25	226.332256	1.802822	22.774 ± 0.013	22.352 ± 0.007	22.006 ± 0.007	0.014 ± 0.001	0.042 ± 0.015

Table C.2: GC candidates identified in MATLAS-2019. The magnitudes are obtained using aperture photometry and are corrected from Galactic Extinction and Encircled Energy. Asterisks indicate the spectroscopically confirmed globular clusters.

Name	RA (J2000.0)	Dec (J2000.0)	F475W (mag)	F606W (mag)	F814W (mag)	R_e (arcsec)	Ellipticity
GC0*	226.336544	1.817503	23.330 ± 0.013	22.883 ± 0.006	22.544 ± 0.006	0.034 ± 0.000	0.096 ± 0.017
GC1*	226.331357	1.815125	23.793 ± 0.020	23.335 ± 0.009	22.933 ± 0.007	0.038 ± 0.001	0.030 ± 0.018
GC2*	226.335160	1.813678	23.576 ± 0.017	23.082 ± 0.007	22.684 ± 0.006	0.037 ± 0.001	0.029 ± 0.018
GC3*	226.334535	1.812961	22.628 ± 0.007	22.181 ± 0.004	21.798 ± 0.004	0.052 ± 0.000	0.089 ± 0.014
GC4*	226.335797	1.813603	24.227 ± 0.031	23.727 ± 0.012	23.320 ± 0.010	0.033 ± 0.001	0.098 ± 0.020
GC5*	226.333920	1.812404	22.999 ± 0.010	22.549 ± 0.005	22.123 ± 0.005	0.042 ± 0.000	0.060 ± 0.016
GC6*	226.329937	1.811504	24.159 ± 0.029	23.634 ± 0.011	23.264 ± 0.009	0.038 ± 0.001	0.149 ± 0.019
GC7*	226.335548	1.812565	24.187 ± 0.030	23.799 ± 0.013	23.359 ± 0.010	0.030 ± 0.001	0.027 ± 0.020
GC8*	226.335655	1.811625	23.438 ± 0.015	22.967 ± 0.007	22.521 ± 0.005	0.043 ± 0.000	0.086 ± 0.017
GC9*	226.333500	1.811074	23.616 ± 0.018	23.171 ± 0.008	22.808 ± 0.006	0.034 ± 0.001	0.045 ± 0.018
GC10*	226.333823	1.810629	23.684 ± 0.019	23.219 ± 0.008	22.799 ± 0.006	0.034 ± 0.001	0.055 ± 0.018
GC11	226.338345	1.818353	25.139 ± 0.070	24.740 ± 0.030	24.345 ± 0.026	0.062 ± 0.002	0.105 ± 0.026
GC12	226.337543	1.817332	24.935 ± 0.058	24.448 ± 0.022	24.053 ± 0.020	0.052 ± 0.001	0.080 ± 0.025
GC13	226.333652	1.815722	25.284 ± 0.079	24.827 ± 0.032	24.473 ± 0.029	0.042 ± 0.002	0.075 ± 0.027
GC14	226.330051	1.814242	24.619 ± 0.043	24.123 ± 0.017	23.677 ± 0.014	0.033 ± 0.001	0.021 ± 0.021
GC15	226.336456	1.815258	23.842 ± 0.021	23.352 ± 0.009	22.900 ± 0.007	0.030 ± 0.001	0.007 ± 0.018
GC16	226.332685	1.813938	25.554 ± 0.102	25.103 ± 0.042	24.757 ± 0.037	0.042 ± 0.003	0.145 ± 0.030
GC17	226.331124	1.813442	24.792 ± 0.051	24.374 ± 0.021	23.894 ± 0.016	0.042 ± 0.001	0.107 ± 0.024
GC18	226.330619	1.812414	24.967 ± 0.060	24.496 ± 0.023	24.086 ± 0.020	0.037 ± 0.002	0.045 ± 0.026
GC19	226.328714	1.811063	24.956 ± 0.059	24.457 ± 0.022	24.036 ± 0.019	0.075 ± 0.001	0.106 ± 0.025
GC20	226.336051	1.812232	25.954 ± 0.145	25.574 ± 0.063	25.100 ± 0.050	0.091 ± 0.004	0.010 ± 0.038
GC21	226.331104	1.810617	24.551 ± 0.041	24.094 ± 0.016	23.697 ± 0.014	0.065 ± 0.001	0.140 ± 0.021
GC22	226.330057	1.810117	24.528 ± 0.040	24.131 ± 0.017	23.704 ± 0.014	0.042 ± 0.001	0.134 ± 0.021
GC23	226.335041	1.810901	24.925 ± 0.057	24.491 ± 0.023	24.108 ± 0.021	0.039 ± 0.002	0.067 ± 0.026
GC24	226.334080	1.810156	24.185 ± 0.030	23.808 ± 0.013	23.456 ± 0.011	0.040 ± 0.001	0.036 ± 0.020
GC25	226.315201	1.804219	24.756 ± 0.049	24.323 ± 0.020	23.893 ± 0.016	0.042 ± 0.001	0.096 ± 0.024
GC26	226.320729	1.796235	22.320 ± 0.006	21.765 ± 0.004	21.359 ± 0.000	0.013 ± 0.000	0.025 ± 0.012
GC27	226.333080	1.802732	23.104 ± 0.011	22.598 ± 0.005	22.163 ± 0.005	0.018 ± 0.001	0.027 ± 0.016
GC28	226.341566	1.803010	25.462 ± 0.094	24.956 ± 0.037	24.590 ± 0.032	0.050 ± 0.002	0.173 ± 0.029
GC29	226.332256	1.802822	22.640 ± 0.008	22.231 ± 0.005	21.894 ± 0.004	0.014 ± 0.000	0.042 ± 0.014